

1 **Chemical characterization of oxygenated organic compounds**
2 **in gas-phase and particle-phase using iodide-CIMS with**
3 **FIGAERO in urban air**

4 Chenshuo Ye¹, Bin Yuan^{2,3,*}, Yi Lin^{2,3}, Zelong Wang^{2,3}, Weiwei Hu⁴, Tiange Li^{2,3}, Wei
5 Chen⁴, Caihong Wu^{2,3}, Chaomin Wang^{2,3}, Shan Huang^{2,3}, Jipeng Qi^{2,3}, Baolin Wang⁵,
6 Chen Wang⁵, Wei Song⁴, Xinming Wang⁴, E Zheng^{2,3}, Jordan E. Krechmer⁶, Penglin
7 Ye⁷, Zhanyi Zhang^{2,3}, Xuemei Wang^{2,3}, Douglas R. Worsnop⁶, Min Shao^{2,3,1}

8 ¹ College of Environmental Sciences and Engineering, Peking University, Beijing
9 100871, China

10 ² Institute for Environmental and Climate Research, Jinan University, Guangzhou
11 511443, China

12 ³ Guangdong-Hongkong-Macau Joint Laboratory of Collaborative Innovation for
13 Environmental Quality, Guangzhou 511443, China

14 ⁴ Guangzhou Institute of Geochemistry, Chinese Academy of Sciences, Guangzhou
15 511443, China

16 ⁵ School of Environmental Science and Engineering, Qilu University of Technology,
17 Jinan 250353, China

18 ⁶ Aerodyne Research, Inc., 45 Manning Rd., Billerica, MA, USA

19 ⁷ Shanghai Key Laboratory of Atmospheric Particle Pollution and Prevention (LAP³),
20 Department of Environmental Science and Engineering, Fudan University, Shanghai
21 200438, China

22 *Correspondence to: byuan@jnu.edu.cn

23

24 **Abstract**

25 The characterization of oxygenated organic compounds in urban areas remains a
26 pivotal gap in our understanding of the evolution of organic carbon under polluted
27 environments, as the atmospheric processes involving interactions between organic and
28 inorganic compounds, anthropogenic pollutants and natural emissions lead to the
29 formation of various and complex secondary products. Here, we describe
30 measurements of an iodide chemical ionization time-of-flight mass spectrometer
31 installed with a Filter Inlet for Gases and AEROSols (FIGAERO-I-CIMS) in both gas-
32 phase and particle-phase at an urban site in Guangzhou, a typical mega-city in southern
33 China, during the autumn of 2018. Abundant oxygenated organic compounds
34 containing 2-5 oxygen atoms were observed, including organic acids, multi-functional
35 organic compounds typically emitted from biomass burning, oxidation products of
36 biogenic hydrocarbons and aromatics. Photochemistry played dominant roles in the
37 formation of gaseous organic acids and isoprene-derived organic nitrates, while
38 nighttime chemistry contributed significantly to the formation of monoterpene-derived
39 organic nitrates and inorganics. Nitrogen-containing organic compounds occupied a
40 significant fraction of the total signal in both the gas and particle phases, with elevated
41 fractions at higher molecular weights. Measurements of organic compounds in particle
42 the phase by FIGAERO-I-CIMS explained $24\pm 0.8\%$ of the total organic aerosol mass
43 measured by aerosol mass spectrometer (AMS), and the fraction increased for more
44 aged organic aerosol. The systematical interpretation of mass spectra of the FIGAERO-
45 I-CIMS in the urban area of Guangzhou provides a holistic view of numerous
46 oxygenated organic compounds in the urban atmosphere, which can serve as a reference
47 for the future field measurements by FIGAERO-I-CIMS in polluted urban regions.

48

49 **1 Introduction**

50 In urban air, atmospheric chemical processes are varied and complex, as the result
51 of large emissions of both anthropogenic pollutants and biogenic volatile organic
52 compounds, associated with strong interactions with each other (He et al., 2014; Karl
53 et al., 2018; Shrivastava et al., 2019). Consequently, strong formation of secondary
54 pollutants, e.g. ozone and secondary organic aerosol (SOA), are observed in urban and
55 downwind regions (Huang et al., 2015; Zhang et al., 2014). Oxygenated organic
56 compounds are not fully accounted for in some earlier studies, which may explain some
57 of the discrepancies between observations and models for many unaddressed issues in
58 atmospheric chemistry. Oxygenated organic compounds are supposed to be the top
59 candidates for missing OH reactivity observed in various environments including
60 pristine rainforests and urbanized areas (Noelscher et al., 2016; Yang et al., 2016, 2017).
61 The photolysis of carbonyls serves as a critical radical source driving ozone formation
62 in highly polluted industrialized areas (Edwards et al., 2014; Liu et al., 2012; Xue et al.,
63 2016). Although it has been discovered a long time ago that oxygenated organic
64 compounds make up a substantial fraction of submicron aerosol mass (Kroll and
65 Seinfeld, 2008), enormous difficulty still exists in accurately predicting formation and
66 evolution of SOA (de Gouw et al., 2005; Hodzic et al., 2010; Volkamer et al., 2006).

67 One of the biggest obstacles to ~~understand~~understanding the role of oxygenated
68 organic compounds is the characterization of these extremely complicated and diverse
69 chemicals which encompass tens of thousands of individual species spanning a wide
70 range of volatility. Chemical ionization mass spectrometry (CIMS) is a powerful
71 technique for the molecular-level characterization of oxygenated organic compounds
72 because of the following advantages (Zhao, 2018): direct measurements and fast time
73 response to capture the rapid temporal change of short-lifetime intermediates; soft
74 ionization providing chemical information on molecular level; selective ionization
75 ensuring measurements for specific classes of species. Iodide anion ionizes species
76 mainly through adduction (Iyer et al., 2016) and is used for the detection of oxygenated
77 organic compounds particularly organic compounds with 2-5 oxygen atoms (Lee et al.,

2014; Lopez-Hilfiker et al., 2016; Riva et al., 2019). It has been shown that I-CIMS is an excellent technique to investigate oxidation processes of volatile organic compounds (VOCs) and formation of SOA (Isaacman-VanWertz et al., 2018). Installed with a thermal desorption inlet that collects and heats aerosol to evaporate organic compounds, e.g. Filter Inlet for Gases and AEROSols (FIGAERO, Lopez-Hilfiker et al., 2014) and Micro Orifice Volatilization Impactor (MOVI-HRT-~~F-CIMS~~, Yatavelli et al., 2012), the CIMS instruments are capable of analyzing particle-phase species and gas-particle partitioning in a semi-continuous way (Stark et al., 2017; Stolzenburg et al., 2018).

Although FIGAERO-CIMS has gained recent popularity in atmospheric chemistry research, much of the published work was done in chambers or in the laboratory (D'Ambro et al., 2017, 2018; Hammes et al., 2019; Lopez-Hilfiker et al., 2015). As for the applications in field campaigns, most work has been mostly performed in forest or rural areas (Huang et al., 2019; Hunter et al., 2017; Lee et al., 2016, 2018b), ~~and systematic analysis of~~ measurements in the urban atmosphere by FIGAERO-CIMS is still limited (Le Breton et al., 2018b). ~~In this study, we present the measurement results using FIGAERO-I-CIMS during~~ Meanwhile, a coordinated campaign in Guangzhou, a megacity in the Pearl River Region of China. We provide an overview of gas-phase and particle-phase oxygenated species detected in the systematic analysis on mass spectra of FIGAERO-I-CIMS during the campaign. CIMS in the ambient air is imperative, for a more holistic view in investigating emissions and chemistry of oxygenated organic compounds using FIGAERO-CIMS. In this study, we present the measurement results using FIGAERO-I-CIMS during a coordinated campaign in Guangzhou, a megacity in the Pearl River Region of China. We describe the experimental design, instrumentation setup, calibration and data processing for the FIGAERO-I-CIMS in the campaign. This work will provide a detailed interpretation of the mass spectra of oxygenated species in both gas-phase and particle-phase. The bulk chemical properties of organic compounds in both gas-phase and particle-phase will also be discussed to provide an overview of organic compounds.

2 Methods

2.1 Measurement site and supporting data

Measurements were conducted during the coordinated campaign “Particles, Radicals and Intermediates from oxidation of primary Emissions over the Great Bay Area” (PRIDE-GBA) in October and November 2018. The Great Bay Area (GBA) refers to a highly industrialized and urbanized area in southern China, including two Special Administrative Regions of Hong Kong and Macao, and nine cities surrounding the Pearl River estuary. Affected by the subtropical monsoon climate, the weather in the region was characterized by high temperatures and relative humidity (RH) as well as sufficient sunshine (~~global~~total solar radiation of the Pearl River Delta region in ~~Fall,~~the fall of 2016 was ~ 1200 MJ/m², Liu et al., 2018). The city of Guangzhou lies in the north of the GBA and south of the mountains. Therefore, the city is extensively influenced by both anthropogenic and biogenic emissions. The urban site was located at Guangzhou Institute of Geochemistry, Chinese Academy of Sciences (23.14°N, 113.36°E). Online instruments sampled from inlets set up in laboratories on the eighth-floor or ninth-floor (about 25 meters above the ground).

In addition to FIGAERO-I-CIMS discussed later, ~~measurements~~measurement data from a suite of other instruments were also used in this work. A high-resolution time-of-flight aerosol mass spectrometer (HR-ToF-AMS, Aerodyne Research, Inc.) was deployed to provide chemical composition and many other parameters of ambient aerosol including f60, liquid water content (LWC), particulate organic ~~nitrates~~nitrate and elemental ratios (Hu et al., 2016, 2018). The parameter f60 is the ratio of the integrated signal at m/z 60 to the total signal of organic components and is used as a tracer for biomass burning emissions (Cubison et al., 2011). LWC of aerosol was taken as the sum of water contributed by inorganic components ~~which was~~ predicted by ISORROPIA II model and organic components ~~which was~~ calculated based on the organic hygroscopicity parameter (Fountoukis and Nenes, 2007; Guo et al., 2015). Based on AMS data, organic nitrate concentrations were determined by 2-3 times lower NO₂⁺/NO⁺ ratios for organic nitrate than inorganic nitrate (Fry et al., 2013). The calculation method of elemental ratios based on AMS data has been described

136 elsewhere (Aiken et al., 2007; Canagaratna et al., 2015). Detailed information about
137 AMS measurements from the PRIDE-GBA campaign is forthcoming in a separate
138 manuscript. An online GC-MS/FID (Wuhan Tianhong Instrument Co., Ltd) and a
139 proton transfer reaction time-of-flight mass spectrometer (PTR-ToF-MS, Ionicon
140 Analytic GmbH) (Yuan et al., 2017) served as the analytical techniques for measuring
141 isoprene and other VOCs (e.g. monoterpenes, aromatics and a few oxygenated VOCs)
142 (Wu et al., 2020), respectively. Trace gases (CO, O₃, NO and NO₂) were measured by
143 commercial gas monitors (Thermo Fisher Scientific Inc.) (Wang et al., 2020d).
144 Photolysis rates were measured by PFS-100 photolysis spectrometer (Focused
145 Photonics Inc.). Temperature and RH were measured by a Vantage Pro2 weather station
146 (Davis Instruments Corp.). Time series and diurnal profiles of meteorological
147 parameters, trace gases, the photolysis rate of NO₂ (j_{NO_2}) along with several important
148 VOCs (isoprene, monoterpenes, toluene and benzene) are shown in [FigureFig. S1](#). The
149 temperature during the campaign was between 17 and 33°C with an average of 24°C
150 and RH was between 27 and 97% with an average of 70%.

151 **2.2 FIGAERO-I-CIMS**

152 **2.2.1 Experimental setup**

153 Our instrument consists of a Filter Inlet for Gases and AEROSols (FIGAERO)
154 and a time-of-flight chemical ionization mass spectrometer coupled with an iodide
155 ionization source (Bertram et al., 2011; Lee et al., 2014; Lopez-Hilfiker et al., 2014).
156 The FIGAERO is a multi-port inlet assembly following a two-step procedure
157 alternating between gas mode in which online measurements of gases and semi-
158 continuous sampling of particle-phase species are conducted, and particle mode in
159 which particulate composition is investigated via thermal desorption (Lopez-Hilfiker et
160 al., 2014; Thornton et al., 2020). Iodide source is a “soft” ionization technique with
161 little ionization-induced fragmentation and selective detection towards multi-functional
162 organic compounds, providing elemental compositions for thousands of oxygenated
163 compounds in the atmosphere (Hyytinen et al., 2018; Iyer et al., 2016; Lee et al., 2014;
164 Riva et al., 2019).

165 The sample air was drawn into the ion molecule reaction (IMR) chamber where
166 it intersected and reacted with ~~the iodide~~primary ions generated by flowing 2 mL/min
167 1000 ppm methyl iodide in 2.4 L/min N₂ through an X-ray source. The pressure in the
168 IMR chamber was maintained at 370-390 mbar. Equipped with a long time-of-flight
169 mass analyzer, our instrument was configured to measure singularly charged ions up to
170 603 Th with a mass resolving power of 10000-11000 ($m/\Delta m$ at 50% height) during the
171 campaign (Fig. S2).

172 Ambient air was continuously sampled through two inlets protruding about 1.5
173 meters out of a window on ninth-floor of a building. One was a 3-meter PFA tubing
174 (1/4-inch OD) for gas phase sampling, through which roughly 9 L/min air was drawn,
175 and 2 L/min was directly taken into the instrument for gas measurements without
176 removing particles, resulting in an inlet residence time of 0.24 seconds. The gas
177 sampling line inside the room was covered by heat insulation associated with a heating
178 cable to minimize condensation on the tubing surface. The other inlet for particle phase
179 was a 3.8-meter metal tubing (3/8-inch OD) fitted with a PM_{2.5} cyclone and a Nafion
180 dryer (Perma Pure, model PD-07018T-12MSS) to reduce water content in the sampled
181 air. The particle phase inlet was drawn by a laminar flow at ~8 L/min (Reynolds number
182 of ~1500), 3.8 L/min of which was collected on PTFE membrane filters (Zefluor[®], Pall
183 Inc., USA). The residence time was 1.3 seconds for the particle phase sampling line.
184 Semi-volatility and low-volatility compounds tend to interact with wall surfaces of both
185 ~~inlet~~inlets and ~~the~~ IMR and thus extend response time (Krechmer et al., 2016). As
186 accurate correction for wall losses remains impossible, no wall loss correction was
187 performed in this study.

188 The FIGAERO worked in a cyclical 1-hour pattern with two modes (Fig. S3):
189 measuring gas for the first 24 minutes while simultaneously collecting particles on the
190 filter; and then analyzing the particle-phase collection for another 36 minutes. In every
191 24-minute gas mode, ambient air was measured for the first 21 minutes, followed by 3-
192 minute gas background by overflowing zero air at 5 L/min through a pinhole just in ~~the~~
193 front of the IMR. The background measurements ~~for CIMS~~ are inevitably influenced
194 by wall interactions, especially for “sticky” species. Recently, Palm et al. (2019)

195 proposed a new way to determine gas background (“fast background”) by fast switching
196 between ambient air and background, which greatly improves accurate determination
197 of CIMS background. In the remaining 36 minutes, the components of the collected
198 particles were thermally desorbed and introduced into the CIMS with 2 L/min N₂ carrier
199 gas. The N₂ flow was ramped from ambient temperature to 175°C in 12 minutes and
200 held for another 20 minutes. Schematic diagram of working modes and temperature
201 profile of FIGAERO heating in a single cycle is shown in Fig. S4. Particle background
202 was determined every 6th 1-hour running cycles in which ambient air passed over a filter
203 (Parker Balston, model 9922-11-CQ) in front of the FIGAERO filter.

204 **2.2.2 Calibration experiments**

205 Using various techniques, we calibrated dozens of chemical compounds in the
206 laboratory. Table S1 summarizes the calibrated species and corresponding calibration
207 methods. (1) Gas cylinders are commercially available for a few species (e.g. chlorine,
208 hydrogen cyanide). The gaseous standards were diluted down to different
209 concentrations and then introduced to the CIMS. (2) For those VOCs of which standards
210 are liquid or solid, solutions with known concentrations are made and then vaporized
211 using the liquid calibration unit (LCU, Ionicon Analytic GmbH) to provide gaseous
212 standards. (3) Commercial permeation tubes are available for some species (e.g. nitric
213 acid). (4) Some gaseous chemicals were generated in the laboratory. For example,
214 isocyanic acid was generated from thermal decomposition of cyanuric acid in a
215 diffusion cell (Li et al., 2021; Wang et al., 2020d), and dinitrogen pentoxide was
216 generated via the reaction of ozone with excess nitrogen dioxide in a flow reactor
217 (Bertram et al., 2009). (5) Compounds of low vapor pressure were calibrated through
218 the FIGAERO (Lopez-Hilfiker et al., 2014). Briefly, certain amounts of target species
219 dissolved in organic solvents (e.g. isopropanol or acetone) were deposited onto the
220 PTFE filter of the FIGAERO using a syringe, and the droplet was then subjected to a
221 temperature-programmed thermal desorption by N₂ gas. The sensitivity ~~for particle~~
222 ~~phase~~ was determined as the integrated signals under thermogram profiles versus the
223 ~~amount~~amounts of deposited calibrant.

224 ~~In addition to sensitivity calibration, the effects of humidity on the sensitivity for~~
225 ~~various species were investigated in the laboratory, some of which are shown in Fig.~~
226 ~~S5. In addition to sensitivity calibration, the effect of humidity on the sensitivity for~~
227 ~~various species was investigated in the laboratory, some of which are shown in Fig.~~
228 ~~S5. Considering water vapor pressure in the IMR, our humidity-dependent curves are~~
229 ~~generally consistent with those reported in Lee et al. (2014) (see detailed discussions in~~
230 ~~Section S3 in the supplement).~~ Low-molecular-weight acids, e.g., formic acid and nitric
231 acid, tend to be more sensitive to the humidity changes than multi-functional
232 compounds. Similar tendency of multi-functional compounds associated with less
233 humidity dependence was also reported in previous work (Lee et al., 2014). Considering
234 water vapor pressure in the IMR, our humidity-dependent curves are generally
235 consistent with those reported in Lee et al. (2014) (see detailed discussions in Section
236 S3 in the Supplement).

237 In the later part of the campaign (after Oct. 22), an isotopically labeled formic
238 acid (DCOOH, Cambridge Isotope Laboratories, Inc.) permeation tube held at constant
239 temperature (65 °C), was mixed with 10 mL/min N₂ and continuously delivered into
240 the entrance of sampling inlet in order to derive a humidity dependence function from
241 the field measurements. DCOOH signals during the campaign exhibited a humidity-
242 dependent curve consistent with formic acid obtained in the laboratory (Fig. S5). We
243 applied humidity correction to the species with the humidity-dependent ~~curve~~curves
244 determined in the laboratory (underlined species in Table S1). For other compounds,
245 humidity correction was not applied, as there is no universal pattern of humidity
246 dependence for all detected species and multi-functional compounds that comprise the
247 majority of the species measured by FIGAERO-I-CIMS are usually less influenced by
248 humidity.

249 The measured concentration of DCOOH was steady after ~~being applied to~~
250 humidity correction was applied (Fig. S6g), indicating the stability of our instrument.
251 In addition, we also performed field calibrations throughout the campaign to check the
252 instrument status by spotting a solution mixture of levoglucosan, heptaethylene glycol
253 and octaethylene glycol ~~on~~onto the FIGAERO filter every 2-3 days (Fig. S6). Multiple-

254 point calibrations for these organic species were performed in the beginning and the
255 end of the campaign. The concentration of the solution used in the first two calibration
256 experiments was too high, so we prepared a new solution for calibrations after
257 November. The relative changes of the determined calibration factors in November
258 were within 50% for the calibrated species.

259 **2.2.3 Data processing**

260 The TofWare software (version 3.0.3; Tofwerk AG, Switzerland) was used to
261 conduct the high-resolution peak fitting for the mass spectra data of ToF-CIMS,
262 including mass calibration, instrumental parameters optimization (peak shape and peak
263 width) and bunch fitting of high-resolution peaks (Stark et al., 2015). In this study, the
264 signals of ions were normalized to the sum signals of I^- and H_2OI^- at 10^6 cps.
265 Hourly particle-phase data were obtained by integrating the signals of various ions
266 during each FIGAERO desorption period. Background corrected signals were obtained
267 by subtracting linearly interpolated background signals from ambient signals (and
268 integrated signals) for ions in the gas (and particle) phase.

269 In order to determine the sensitivities of uncalibrated species, voltage scanning
270 procedure was performed from time to time throughout the campaign covering different
271 times of the day (Iyer et al., 2016; Lopez-Hilfiker et al., 2016). Here, we selected four
272 representative periods including morning, afternoon, evening and night on polluted
273 days. By performing sigmoidal fitting on the remaining signals as a function of voltages,
274 a dV_{50} value of each ion from each period was determined at which voltage half of one
275 kind of ion dissociated (Lopez-Hilfiker et al., 2016). We observed a positive correlation
276 between the sensitivities of the ions relative to maximum sensitivity and their average
277 dV_{50} values (Fig. S7), consistent with previous studies (Isaacman-VanWertz et al., 2018;
278 Lopez-Hilfiker et al., 2016). This relationship was used to calculate response factors for
279 uncalibrated species, after taking into account the relative transmission efficiency for
280 the ions (see Section S1 in the Supplement for detailed analysis).

281 **3 Results and discussion**

282 **3.1 Overview of detected species in the mass spectra**

283 We identify 1334 ions adducted with iodide from the mass spectra, among which
284 427 are charged closed-shell organic compounds containing only C, H, O elements
285 ($C_xH_yO_zI^-$) and 388 are charged closed-shell organic compounds containing C, H, O
286 and N elements ($C_xH_yN_{1,2}O_zI^-$). For species with the formula of $C_xH_yO_z$, x ranges
287 from 1 to 20; y is an even number and no more than $2x+2$; z is greater than or equal to
288 2. The range of carbon number x for the ions with $C_xH_yN_{1,2}O_z$ is the same as the ions
289 with $C_xH_yO_z$. For species containing one nitrogen ($C_xH_yNO_z$), y is an odd number and
290 less than $2x+2$; z is larger than or equal to 2. For species containing two nitrogen atoms
291 ($C_xH_yN_2O_z$), y is an even number and less than $2x+1$; z is larger than or equal to 4.
292 Table 1 summarizes species discussed in the main text. Although ~~iodide~~iodide clusters
293 with two nitrogen atoms and zero nitrogen atoms both lie on odd masses, they can be
294 separated for certain ions with the current resolving power, as demonstrated by the peak
295 fitting results of mass spectrum at m/z 311 (Fig. S8).

296 The campaign-averaged mass spectra of detected ions in the both gas and particle
297 phases are shown in Fig. 1. In general, molecules in particle-phase have larger
298 molecular weights compared to those in gas-phase compounds. Signals in the mass
299 range of 150—300 Th comprise a large fraction of gas-phase compounds, and
300 concentrations in the gas phase decrease quickly with m/z higher than 250 Th. In
301 contrast, the detected signals in the particle phase are mainly distributed within the
302 range of 200-320 Th.

303 ~~We compare the concentration for various ions between the Average nighttime~~
304 ~~(10 pm - 6 am) and daytime (10 am - 6 pm) and nighttime (10 pm—6 am), by~~
305 ~~determining concentration~~mixing ratios ~~between at night and during the daytime (for~~
306 ~~various species were shown in Fig. 2).~~ Most species have higher concentrations during
307 the daytime, especially for relatively volatile compounds in gas-phase, despite the fact
308 that lower boundary layer height at night should increase nighttime ~~mixing~~
309 ~~ratios~~concentration, as ~~behaved for~~ many primary gases behaved, e.g. CO (Fig. S1) (Wu
310 et al., 2020). The higher concentrations during the daytime for most species detected
311 by FIGAERO-I-CIMS suggest the dominant role of photochemical induced oxidation
312 in forming these oxidized compounds. In addition to typical nocturnal species including

313 nitryl chloride ($ClNO_2I^-$), chlorine nitrate ($ClONO_2I^-$) and dinitrogen pentoxide
314 ($N_2O_5I^-$), higher concentrations for the ions of $C_6H_{10}O_5I^-$ and $C_6H_{12}O_5I^-$ were
315 also observed, which will be discussed in [the](#) next section. A large number of particulate
316 N-containing organic compounds increase [during the at](#) night as well, as shown by mass
317 defect diagrams of $C_xH_yO_z$ and $C_xH_yN_{1,2}O_z$ color coded by the night to day ratios
318 (Fig. S9).

319 Based on the mass spectra shown in Fig. 1, we identify a number of ions
320 associated with high concentrations in both gas and particle phases. In the following
321 Section 3.2-3.7, we will perform interpretation of the mass spectra by analyzing
322 variability and correlation of these important ions, including monosaccharide-derived
323 compounds (with brown tags in Fig. 1), oxygenated aromatics (with purple tags),
324 organic acids (with pink tags), oxidation products of biogenic volatile organic
325 compounds (BVOCs, with green tags), sulfur-containing compounds, and inorganics
326 (with blue tags). After going through detailed analysis [in at](#) the species level, Section 3.8
327 will provide an overall picture about bulk chemical characteristics of detected organic
328 compounds in terms of the distributions of average carbon oxidation states, carbon
329 number and oxygen number. Lastly, Section 3.9 will compare our measurement of
330 organic aerosol (OA) with AMS data.

331 **3.2 Monosaccharide-derived compounds**

332 $C_6H_{10}O_5$ and $C_6H_{12}O_5$ are highly correlated with each other in aerosol ($r=0.92$),
333 and they are two of [at the](#) few $C_xH_yO_z$ compounds with higher concentrations at night.
334 Previous work assigned them as monosaccharide derived compounds emitted from
335 biomass burning (Bhattacharai et al., 2019; Qi et al., 2019; Reyes-Villegas et al., 2018;
336 Simoneit et al., 1999).

337 In this campaign, $C_6H_{10}O_5$ was detected mostly in the particle phase (the fraction
338 in the particle phase $F_p=0.81\pm 0.09$) with an average concentration of 0.073 ± 0.076
339 $\mu\text{g}/\text{m}^3$. Its diurnal profile started increasing [during at](#) dusk, reaching a peak at about
340 midnight and then fell off, as shown in Fig. 3. The mass fraction of $C_6H_{10}O_5$ in OA had
341 a similar diurnal profile, and the ratios of $C_6H_{10}O_5$ to CO increased at night (from

342 0.17±0.02 to 0.5±0.03 $\mu\text{g}\cdot\text{m}^{-3}/\text{ppm}$, Fig. 3c), both suggesting enhanced emissions of
343 this compound were related with combustion activities ~~during~~ in the evening, e.g.,
344 residential biofuel burning for cooking as reported by some previous measurements in
345 China (Wang et al., 2020c; Zhang et al., 2015). Furthermore, the time variations of
346 particle-phase $\text{C}_6\text{H}_{10}\text{O}_5\text{I}^-$ were very similar to ~~that those~~ of the m/z 60 fragment in
347 AMS mass spectra (Fig. 3a), which is an identified tracer of biomass burning OA
348 produced from the thermal decomposition of levoglucosan and similar compounds
349 ~~during detection by on the vaporizer of~~ AMS (Brege et al., 2018; Cubison et al., 2011;
350 Schneider et al., 2006). Therefore, $\text{C}_6\text{H}_{10}\text{O}_5$ was probably levoglucosan and its isomers
351 (mannosan and galactosan), and $\text{C}_6\text{H}_{12}\text{O}_5$ was probably also a similar monosaccharide
352 compound ~~emitted from biomass burning that had similar sources to $\text{C}_6\text{H}_{10}\text{O}_5$.~~

353 3.3 Oxygenated aromatic compounds

354 Combustion activities emit a great deal of compounds besides saccharides that
355 the I-CIMS instrument can detect including nitro-aromatics and guaiacol derivatives
356 (Gaston et al., 2016; Kong et al., 2021). Nitro-benzenediols ($\text{C}_6\text{H}_5\text{NO}_4\text{I}^-$) as well as
357 the highly correlated homologue methyl nitro-benzenediols ($\text{C}_7\text{H}_7\text{NO}_4\text{I}^-$) ($r=0.88$ in
358 the particle phase), exhibited double peaks in their diurnal profiles (Fig. 4).
359 ~~Concentrations of $\text{C}_6\text{H}_5\text{NO}_4$ and $\text{C}_7\text{H}_7\text{NO}_4$ were enhanced~~ One was in the evening,
360 similar to levoglucosan ($\text{C}_6\text{H}_{10}\text{O}_5$). ~~Another concentration~~ The other peak was at noon
361 ~~was also observed for $\text{C}_6\text{H}_5\text{NO}_4$ and $\text{C}_7\text{H}_7\text{NO}_4$.~~ The scatterplot of $\text{C}_6\text{H}_5\text{NO}_4$ as the
362 function of $\text{C}_6\text{H}_{10}\text{O}_5$ exhibits two different slopes (Fig. 5): the lower slope at night
363 (0.088 ± 0.005) indicates the contribution of biomass burning, while the higher slope
364 during the daytime (0.26 ± 0.02) suggests there were other important sources for nitro-
365 aromatics, potentially secondary formation from photooxidation of aromatics (Jenkin
366 et al., 2003). Guaiacol derivatives may have similar sources with nitro-aromatics, as
367 implied by the resemblance of the scatterplots of these two chemical classes versus
368 levoglucosan (cf., Fig. S10 and Fig. 5).

369 Nitrophenols ($\text{C}_6\text{H}_5\text{NO}_3\text{I}^-$), methyl nitrophenols ($\text{C}_7\text{H}_7\text{NO}_3\text{I}^-$) and
370 dinitrophenols ($\text{C}_6\text{H}_4\text{N}_2\text{O}_5\text{I}^-$) were the most significant components of nitro-aromatics

371 in the gas phase. Despite the fact that nitrated phenols could be formed by
372 photochemical oxidation ~~from~~of their aromatic hydrocarbon precursors (Wang et al.,
373 2020a; Yuan et al., 2016), none of them peaked in the daytime, consistent with a
374 previous proposal on photolysis as ~~the~~ dominant ~~chemical-loss pathway~~ for these
375 compounds (Chen et al., 2011; Yuan et al., 2016). ~~Nitrophenols~~ $C_6H_5NO_3$ and ~~methyl~~
376 ~~nitrophenols~~ $C_7H_7NO_3$ peaked in the evening, suggesting ~~either important contributions~~
377 ~~of~~ NO_3 -~~oxidation-induced reactions and/~~or primary emissions ~~was important sources.~~
378 ~~It is interesting to observe that the.~~ The peak ~~concentration for~~time of $C_6H_4N_2O_5$ was
379 later than ~~the nitrophenols~~that of $C_6H_5NO_3$, in agreement with dinitrophenols as the
380 oxidation products from nitrophenols (Harrison et al., 2005).

381 ~~Several ions~~We also detected non-N-containing compounds that were identified
382 as oxidation products of aromatics in the literature, including $C_7H_6O_4I^-$, $C_7H_8O_4I^-$
383 and $C_7H_8O_5I^-$ (Mehra et al., 2020; Schwantes et al., 2017), ~~were detected during the~~
384 ~~campaign.~~ $C_7H_6O_4$ and $C_7H_8O_4$ correlated well with each other ($r=0.72$ in gas-phase
385 and 0.91 in particle-phase). High concentrations of $C_7H_6O_4$ and $C_7H_8O_4$ were mainly
386 observed during the periods with lower NO_x concentration, which was a contrast to the
387 variations of nitrophenols (Fig. S10). ~~We observed~~In addition, the concentration ratios
388 of $C_7H_8O_4I^-$ and $C_7H_7NO_3I^-$ ~~were~~are lower for higher NO_x
389 ~~concentrations~~concentration (Fig. 5), consistent with the literature that the formation of
390 $C_7H_6O_4$ and $C_7H_8O_4$ is suppressed at high NO_x ~~concentrations~~concentration
391 (Schwantes et al., 2017). $C_7H_8O_5$ ~~was~~is reported as the ring-retaining oxidation product
392 of $C_7H_8O_4$ which is a typical oxidation product of toluene and cresol (Schwantes et al.,
393 2017; Wang et al., 2020b), as well as the ring-scission products of aromatic
394 hydrocarbons with more carbon atoms, e.g. trimethyl benzenes (Mehra et al., 2020).
395 Given that $C_7H_8O_5$ closely followed with $C_7H_8O_4$ ($r=0.93$ in particles), toluene
396 oxidation was probably the main contributor to this ~~ion~~compound.

397 **3.4 Organic acids and related compounds**

398 Organic acids were one of the most abundant species classes detected by I-CIMS
399 (Fig. 1). Low-molecular-weight organic acids (e.g., formic, acetic, glycolic and pyruvic

400 acid) constituted a significant fraction of signals in the mass spectra ~~detected from of~~
401 ~~the~~ gas phase. As shown in Fig. 6 (and also Fig. S11), they had very similar temporal
402 trends with diurnal maxima in the afternoon, indicating photochemical oxidation played
403 a dominant role in their formation (de Gouw et al., 2018; Yuan et al., 2015).

404 In contrast to monocarboxylic acids, dicarboxylic acids partitioned mostly to
405 particle-phase. As the dominant dicarboxylic acids in aerosol (Kawamura and Bikkina,
406 2016; Mellouki et al., 2015), $94\pm 5\%$ and $74\pm 13\%$ (mean \pm one standard deviation of
407 F_p) of $C_2H_2O_4$ and $C_3H_4O_4$, assigned as oxalic and malonic acid, were found in particle-
408 phase, respectively. The concentrations of $C_4H_6O_4$ were significantly lower compared
409 to ~~that of~~ C2 and C3 homologous series, but $C_5H_8O_4$ and $C_6H_{10}O_4$ had unexpected
410 ~~higher~~ high abundance (Fig. 7). Additionally, $C_5H_8O_4$ and $C_6H_{10}O_4$ had considerable
411 fractions in the gas phase ($45\pm 13\%$ and $43\pm 11\%$), significantly higher than their C2-C3
412 homologous series. These two compounds were correlated well with each other in
413 temporal variations ($r=0.97$ and 0.91 in the gas and particle phases, respectively), and
414 their diurnal variations were different from those of oxalic and malonic acid (Fig. 6).
415 Therefore, dicarboxylic acids may not be the dominant contributing species for the two
416 ~~ions~~ compounds. $C_5H_8O_4$ and $C_6H_{10}O_4$ have been observed from previous ~~study~~ studies
417 on isoprene oxidation (Berndt et al., 2018, 2019), attributing them as epoxy
418 hydroperoxyl carbonyl and accretion product, respectively. However, the relative
419 contributions from these possibilities remain unclear.

420 In addition to the series of $C_nH_{2n-2}O_4$ (i.e. $C_2H_2O_4$, $C_3H_4O_4$), we also observed
421 comparable concentrations of $C_nH_{2n-4}O_4$ ~~ions~~ series, especially for carbon number of
422 4 and 5 ($C_4H_4O_4$ and $C_5H_6O_4$). Considering the double bonds in the molecules,
423 $C_nH_{2n-4}O_4$ should be more reactive than $C_nH_{2n-2}O_4$, suggesting there were large
424 sources for these compounds. Previous studies have reported photo-oxidation of
425 aromatics can generate $C_nH_{2n-4}O_4$, including $C_4H_4O_4$ and $C_5H_6O_4$ (Brege et al., 2018;
426 Kawamura et al., 1996; Kawamura and Bikkina, 2016). Our measurements showed that
427 temporal trends of $C_4H_4O_4$ and $C_5H_6O_4$ followed well with those of aromatic
428 hydrocarbons (Fig. S11b), and thus oxidation of aromatics could be an important
429 contributor to $C_nH_{2n-4}O_4$ in the urban air.

3.5 Oxidation products of Biogenic VOCs (BVOCs)

In addition to high anthropogenic emissions of aromatics, terrestrial vegetations nearby also released significant amounts of biogenic VOCs (BVOCs) (Wu et al., 2020). During the campaign, the concentrations of isoprene at noon were between 0.1 and 1.5 ppb, whereas the range of daily maxima of monoterpenes was 0.05-2.5 ppb. Hence, a number of oxidation products of BVOCs were detected (Fig. 8 and Fig. S12).

The ion $C_4H_7NO_5I^-$ was the most abundant N-containing C4 organic compounds that were detected in the gas phase. Its daily maxima occurred in the afternoon and correlated moderately with methyl vinyl ketone (MVK) + methacrolein (MACR) measured by PTR-ToF-MS (Fig. 88b, $r=0.58$). We consequently assigned $C_4H_7NO_5$ as MVK nitrates and MACR nitrates, which waswere reported as the second generation of organic nitrates formed from the oxidation of isoprene hydroxynitrates by OH in the presence of NO_x (Fisher et al., 2016; Paulot et al., 2009). Strong correlations were observed between $C_5H_9NO_4I^-$, $C_5H_9NO_5I^-$ and $C_4H_7NO_5I^-$ ($r=0.93$ and 0.80 , respectively), which was in accordance with their similar formation pathways (Jacobs et al., 2014; Wennberg et al., 2018; Xiong et al., 2015). Hence, we expectexpected these three compounds arewere common oxidation products of isoprene in the polluted atmosphere. While in aerosol, 2-methylglyceric acid ($C_4H_8O_4$) is a commonly reported oxidation product of isoprene formed in high- NO_x conditions (Surratt et al., 2010). We observed the corresponding ion $C_4H_8O_4I^-$ contributing to OA especially in dry conditions with strong sunlight (Fig. S13). This evidence indicates that isoprene oxidation may contribute to $C_4H_8O_4$, but potential contribution from other sources cannot be ruled out in urban areas.

In terms of monoterpenes, a reasonable correlation (Fig. S14a, $r=0.63$) was found between the ions $C_{10}H_{16}O_3I^-$ and $C_{10}H_{16}O_2H^+$ measured by PTR-ToF-MS. $C_{10}H_{16}O_2H^+$ was attributed to pinonaldehyde formed from the oxidation of monoterpenes (Glasius et al., 2000; Larsen et al., 2001; Mutzel et al., 2016). Therefore, we tentatively assign ~~$C_{10}H_{16}O_3$~~ $C_{10}H_{16}O_3I^-$ as pinonic acid and its oxocarboxylic acid isomers, which are formed via the oxidation of pinonaldehyde (Fang et al., 2017).

459 $C_8H_{13}NO_6$ also exhibited enhanced gas-phase formation during the day as pinonic acid
460 did. The correlation coefficient of the two compounds (\oplus) was 0.71. In contrast to other
461 monoterpene nitrates, particle-phase $C_8H_{11}NO_7$ and $C_{10}H_{15}NO_6$ peaked at night and
462 decreased during the daytime (Fig. S12), indicative of the role of NO_3 in producing
463 organic nitrates as reported in the literature (Faxon et al., 2018). However,
464 ~~$C_{10}H_{15}NO_6I^-$~~ $C_{10}H_{15}NO_6I^-$ in the gas phase showed a distinct diurnal profile with peak
465 before the noon. Two possible types of compounds were proposed for $C_{10}H_{15}NO_6$ in
466 previous studies: peroxyacetyl nitrate from pinonaldehyde (Faxon et al., 2018; Nah et
467 al., 2016; Schwantes et al., 2020), or organic nitrates (Bean and Hildebrandt Ruiz, 2016;
468 Boyd et al., 2015). Given the distinct diurnal profiles of $C_{10}H_{15}NO_6I^-$ in the gas and
469 particle phases and the fact that peroxyacetyl nitrate is supposed to dissociate during
470 the FIGAERO heating (Slusher et al., 2004), we speculate that both compounds
471 contributed to this ion. As shown in Fig. S15, $C_8H_{12}O_4$ and $C_9H_{14}O_4$ existed mostly in
472 particle-phase ($F_p=0.63\pm 0.11$ and 0.67 ± 0.10 , respectively). We ~~interpreted~~ interpret
473 them as products of monoterpenes via photochemical processes, consistent with the
474 interpretations presented in previous work (Mohr et al., 2013; Mutzel et al., 2015).

475 **3.6 S-containing compounds**

476 Organosulfates are concerned as important components of SOA (Hallquist et al.,
477 2009; Surratt et al., 2007), and they can be detected by iodide anion via proton
478 abstraction (Le Breton et al., 2018b; Lee et al., 2014). We detected the ion $C_2H_3SO_6^-$
479 with a diurnal peak ~~concentration~~ in the afternoon (Fig. 9). ~~We~~ This ion was attributed
480 ~~$C_2H_3SO_6^-$~~ to glycolic acid sulfate, as suggested by previous work (Galloway et al.,
481 2009; Liao et al., 2015).

482 Abundant SO_3I^- was detected in particles, and it correlated well with the ion
483 $C_2H_3SO_6^-$ (Fig. 9b) and sulfates measured by AMS (Fig. S16). Previous work observed
484 the sulfite ion radical ($\cdot SO_3^-$) during the ionization of organosulfates in a liquid
485 chromatography-electrospray ionization-tandem mass spectrometer (Huang et al.,
486 2018). As a result, the ion SO_3I^- ~~ion~~ from FIGAERO-I-CIMS might be a potential

487 indicator for the total organosulfates. However, more future work is needed for
488 evaluating this possibility.

489 Other sulfate-related ions during gas-phase modes were also detected including
490 HSO_4^- (sulfuric acid), $CH_3SO_3^-$ (methanesulfonic acid) which were enhanced in the
491 gas phase during the daytime, in agreement with the notions of **photochemically**
492 **photochemistry**-induced gas-phase oxidation (Brandt and van Eldik, 1995). However,
493 these data were not available for quantification given that these low-volatile species
494 would condense on our long gas sampling inlet. It should be noted that measuring
495 sulfuric acid in the gas-phase is difficult and generally requires a “wall-less” source
496 design (Eisele and Tanner, 1993).

497 **3.7 Inorganic compounds**

498 There is a growing interest in N_2O_5 and its product nitryl chloride ($ClNO_2$)
499 because $ClNO_2$ is found to serve as a nocturnal reservoir of Cl radical and reactive
500 nitrogen, and hence enhance the ozone formation **the** next day (Osthoff et al., 2008;
501 Wang et al., 2016). Time series of N_2O_5 and $ClNO_2$ exhibited two patterns. During most
502 of the nights, N_2O_5 started to increase quickly at sunset and lasted for only 2-3 hours,
503 and $ClNO_2$ increased in the meantime and ultimately reached its maximum at night,
504 indicative of local formation of $ClNO_2$. However, sometimes a high level of N_2O_5 did
505 not lead to an increase in $ClNO_2$ (tinted background in Fig. 10a), probably due to the
506 lack of chloride salts on the aerosol. Other nocturnal species including $ClONO_2$ and Cl_2
507 were highly correlated with $ClNO_2$ as ~~we~~ expected ($r=0.92$ and 0.83 , respectively),
508 suggesting they had common formation mechanisms (Liu et al., 2017).

509 HNO_3I^- was observed as one of the most abundant species in the mass spectra
510 of FIGAERO-I-CIMS ~~in~~ both **in the** gas and particle **phasephases**. In the gas phase, the
511 ion HNO_3I^- from I-CIMS has been used to quantify nitric acid (Lee et al., 2018a).
512 The concentrations of gas-phase nitric acid peaked in the afternoon, suggesting
513 photochemistry in the daytime as the dominant source for gas-phase nitric acid.

514 Previous study suggested that HNO_3I^- from particle-phase measurement by
515 FIGAERO-I-CIMS can be indicative of nitrate in the particle phase (Lee et al., 2016).

516 Here, the concentrations of HNO_3I^- in the particle phase were compared with
517 particulate nitrate measured by AMS (Fig. 11c). Strong correlation was observed
518 ($r=0.93$), but the concentrations measured by FIGAERO-I-CIMS were higher
519 (slope=1.6), especially for higher concentrations of organic nitrates. Using a threshold
520 of $1 \mu\text{g}/\text{m}^3$ for organic nitrates, the slopes and correlations were higher for the data
521 points with particulate organic nitrates larger than $1 \mu\text{g}/\text{m}^3$ (slope=1.8, $r=0.94$) than
522 those ~~with less than $1 \mu\text{g}/\text{m}^3$ of organic nitrates~~ (slope=1.1, $r=0.90$). In short, our
523 measurements suggest that HNO_3I^- in the particle phase from FIGAERO-I-CIMS are
524 formed from thermal-decomposition of both inorganic ~~nitrates~~nitrate (e.g. NH_4NO_3)
525 and organic nitrates.

526 **3.8 Bulk chemical properties of detected organic compounds**

527 The above discussions on individual chemical groups provide insights into the
528 identification of the mass spectra from FIGAERO-I-CIMS, along with sources and
529 chemistry of oxygenated organic compounds in the urban atmosphere. In this section
530 and the following one, we will provide a bulk analysis of the detected organic
531 compounds.

532 ~~The composition of organic~~Organic compounds detected by FIGAERO-I-CIMS
533 ~~was were~~ comprehensively characterized with detailed elementary composition in
534 $\overline{OS}_C - n_C$ space (Fig. 12) which depicts the average oxidation states of carbon for
535 closed-shell $C_xH_yO_z$ and $C_xH_yN_{1,2}O_z$ compounds ~~clustered with iodide~~ as a function
536 of carbon number. The details in calculation of \overline{OS}_C can be found in Section S2 in SI.
537 S-containing compounds were omitted given their negligible variety and concentration
538 compared to ~~the former two chemical classes ($C_xH_yO_z$ and $C_xH_yN_{1,2}O_z$)~~. The
539 average \overline{OS}_C in the particle phase was higher than that in the gas phase at the same
540 carbon number, especially for carbon number between 2 and 10. This agrees with our
541 expectation that more oxidized compounds would partition more strongly in aerosol, as
542 indicated by larger fractions in particles (Fp) for higher \overline{OS}_C . In addition, the average
543 \overline{OS}_C generally increased for lower carbon number, as a result of functionalization and
544 fragmentation during VOCs aging. However, there was a notable exception in C5 which

545 had a significantly reduced \overline{OS}_C , probably as the result of emissions of isoprene. The
546 analysis of the $\overline{OS}_C - n_C$ space indicates that the large number of organic compounds
547 measured by FIGAERO-I-CIMS are useful to characterize the evolution of organic
548 compounds in the atmosphere.

549 The distributions of carbon ~~number~~ and oxygen ~~number in the numbers of~~ organic
550 compounds ~~measured by FIGAERO-I-CIMS~~ were also investigated, as shown in Fig.
551 13. Most abundant organic compounds measured by FIGAERO-I-CIMS were C2-C3
552 compounds, which accounted for about 66% ~~of organic compounds in the~~ gas-phase
553 and 56% in ~~the~~ particle-phase. It is unexpected that C2-C3 compounds made up such
554 a significant portion ~~of~~ in the particle phase, indicating a non-negligible role of thermal
555 decomposition from low volatility compounds such as accretion products or extremely
556 low volatile organic compounds which were reported from FIGAERO measurements
557 on SOA (D'Ambro et al., 2018; Lopez-Hilfiker et al., 2014; Stark et al., 2017). Organic
558 compounds with carbon numbers over 5 constituted only 3% in the gas phase, while
559 they accounted for 30% in the particle phase. The ~~oxygen numbers of the~~ majority of
560 gaseous organic compounds were ~~associated with no more than 3 oxygen atoms.~~
561 Organic compounds containing ~~2-3~~ 3 oxygen atoms had the largest contribution in both
562 gas-phase (96%) and particle-phase (56%). $C_xH_yN_{1,2}O_z$ accounted for less than 10%
563 of the total oxygenated organic compounds. In the gas phase, compounds with 5-6
564 oxygen atoms accounted for 51% of $C_xH_yN_{1,2}O_z$, indicative of the high levels of
565 organic nitrates in the urban atmosphere. Nitrophenols also contributed significantly to
566 $C_xH_yN_{1,2}O_z$ compounds, as they accounted for 74% of $C_xH_yN_{1,2}O_z$ containing 3
567 oxygen atoms, which in turn contributed to 22% of $C_xH_yN_{1,2}O_z$. In contrast, in the
568 particle phase, the oxygen ~~number numbers~~ of $C_xH_yN_{1,2}O_z$ distributed relatively
569 evenly, as the fractions of compounds with 3-8 oxygen atoms were similar (between
570 12% and 19%). Compared to measurements in a forest in the southeastern United States
571 (cf., Table S1 from Lee et al., 2016), the fractions of N-containing organic compounds
572 with less than 5 oxygen atoms were significantly larger in our measurements as a result
573 of higher concentrations of nitro-aromatics.

574 We further ~~determined~~determined the fractions of N-containing organic
575 compounds in total organic compounds as a function of m/z. It is clear that the observed
576 fractions of N-containing organic compounds ~~are~~were higher for elevated m/z (Fig. 14)
577 and N-containing ions commonly ~~dominated~~dominated at even nominal masses (Fig.
578 S17). The gas-phase CHON ions within the m/z range ~~from of~~250 to 350 Th accounted
579 for about half of the organic compounds in this range. The fractions of CHON ions in
580 particle-phase ~~are~~were somewhat smaller than those in the gas phase ~~for~~within the
581 above m/z ~~of 250-350 Th~~range, but ~~are~~were comparable for higher m/z. A possible
582 explanation for this is that functional groups of nitrate and nitro reduce less in vapor
583 pressure for organic compounds than functional groups of carboxylic ~~acid~~ or oxygen-
584 equivalent hydroxyl ~~that without nitrogen atom do~~ (Capouet and Müller, 2006;
585 Nannoolal et al., 2008; Pankow and Asher, 2008). Consequently, CHON compounds
586 are generally more volatile than CHO compounds with similar molecular weights.

587 In the end, we determined the total concentration of N-containing organic
588 compounds in the particle-phase measured by FIGAERO-I-CIMS and compared it with
589 the particulate organic nitrates derived from AMS (Fig. 15). Good agreement was
590 achieved when the ~~concentrations~~concentration of inorganic nitrate ~~were~~was relatively
591 ~~lower~~low, e.g. below 8 $\mu\text{g}/\text{m}^3$. However, the discrepancies increased when inorganic
592 nitrate ~~were~~higherconcentration increased, which can affect the determination of
593 organic nitrate from AMS. This encouraging result indicates that FIGAERO-I-CIMS is
594 able to capture the variability of organic nitrates in the urban atmosphere, which can be
595 helpful in understanding the sources and formation mechanism of these ~~organic~~
596 nitratescompounds.

597 **3.9 Organic aerosol measurements**

598 The total ~~concentrations~~concentration of organic compounds in the particle phase
599 measured by FIGAERO-I-CIMS ~~were~~was determined and compared with
600 measurements of OA by AMS. The total organic compounds measured by FIGAERO-
601 I-CIMS explained $24 \pm 0.8\%$ (fitted slope \pm one standard deviation) of the total OA in
602 average (Fig. 16a), which is lower than the average fractions ($\sim 50\%$) reported

603 previously in boreal and temperate forests (Lopez-Hilfiker et al., 2016; Stark et al.,
604 2017). The lower fractions determined here might be ~~as~~ the result of larger contributions
605 to OA from primary emissions in ~~the~~ urban air, which are composed of ~~a~~ large number
606 of compounds with little ~~signals~~ in I-CIMS (Zhao et al., 2016). As shown in Fig.
607 16a, organic compounds measured by FIGAERO-I-CIMS ~~account~~ accounted for higher
608 fractions in OA concentrations by AMS for more aged OA, ~~which is~~ consistent with the
609 fact that I-CIMS are more sensitive to oxygenated organic compounds with multiple
610 functional groups (Lee et al., 2014; Lopez-Hilfiker et al., 2016). Furthermore, we expect
611 this fraction to change with the relative contributions of primary emissions and
612 secondary formation for organic compounds in the atmosphere. Similar trends were
613 found in Le Breton et al. (2019), in which an acetate source was used. Acetate ions have
614 been reported to selectively ionize highly oxygenated organic compounds as an iodide
615 source does (Aljawhary et al., 2013).

616 Comparison of the Van Krevelen ~~diagram~~ diagrams between FIGAERO-I-CIMS
617 and AMS also provides useful insights on the measurement of organic compounds in
618 OA. The Van Krevelen diagram has been used as a tool for analyzing functional groups
619 and OA aging by plotting H/C ratios versus O/C ratios (Heald et al., 2010; Lambe et al.,
620 2012). As shown in Fig. ~~16a~~ 16b, the data points ~~for~~ of the bulk OA from FIGAERO-I-
621 CIMS ~~follow~~ followed the same trend as the data points from AMS. However, the bulk
622 OA measured by FIGAERO-I-CIMS only occupied a much smaller region with ~~the~~ O/C
623 ~~ratios~~ between 0.7 and 1.0. We further ~~plot~~ plotted all of the organic compounds in
624 the H/C versus O/C space color-coded with their campaign-average concentrations (Fig.
625 S18a). We ~~observe~~ observed that most ~~particle-phase concentrations measured by data~~
626 ~~points from~~ FIGAERO-I-CIMS distributed across the zone between the slope of 0 and
627 -1.0. These observations provide additional evidence that FIGAERO-I-CIMS may only
628 measure the more oxidized organic compounds in OA.

629 The correlation coefficients between the particle-~~phase~~ concentrations at unit
630 masses by FIGAERO-I-CIMS and OA mass concentration by AMS ~~are~~ were calculated
631 (Fig. S18b). The correlation coefficients ~~are~~ were small for ions below m/z 200, as these
632 ions ~~contribute~~ contributed little to organic aerosol. Moderate and strong correlations

633 ($r > 0.7$) were observed for the ions of m/z between ~~m/z~~ 200 and ~~m/z~~ 400 Th, implying
634 that organic compounds with molecular ~~weightweights~~ of 100-300 g/mol may account
635 for significant fractions in organic aerosol. The possible reason for the lower
636 correlations ~~effor~~ heavier compounds ($m/z > 400$ Th) with OA mass loadings is that
637 these compounds might be related to specific sources or certain chemical processes,
638 which might not contribute at large fractions to the total OA concentration.

639 **4 Summary**

640 We deployed a FIGAERO-I-CIMS instrument to measure oxygenated organic
641 compounds in both gas phase and particle phase at a representative urban site in China.
642 ~~The mass spectra measured by FIGAERO-I-CIMS was systematically interpreted. We~~
643 ~~detected high concentrations of several monosaccharide species (e.g., levoglucosan)~~
644 ~~potentially emitted from biomass burning, which also contributed to the enhancement~~
645 ~~of multiple nitro-aromatic species. Photochemistry was also identified as~~The
646 experimental design and instrumentation setup were described in detail, which goes
647 above and beyond typical studies, including (1) performing sensitivity calibrations in
648 the laboratory using multiple methods for multiple species; (2) performing voltage
649 scanning for unknown compounds detected in the ambient air; (3) performing humidity
650 calibrations for multiple types of species, which we have not seen anyone do after Lee
651 et al. (2014).

652 From the mass spectra, a number of important compounds in the urban
653 atmosphere were identified. We detected high concentrations of several
654 monosaccharide species (e.g., levoglucosan). They were potentially emitted from
655 biomass burning which also contributed to the enhancement of many nitro-aromatic
656 species. Photochemistry was also found to be a strong source of nitro-aromatics. Low-
657 molecular-weight organic acids were mainly observed in the gas phase, and
658 observations ~~support~~supported daytime photochemistry as the dominant source.
659 Different diurnal profiles for various BVOC-derived organic nitrates were observed,
660 reflecting their different formation pathways related to NO_x chemistry (i.e. daytime
661 photo-oxidation, nocturnal NO₃ reactions). Local formation of nitryl chloride was

662 observed, highlighting the potential importance of nighttime chemistry in the urban
663 region.

664 Our measurements show that oxygenated organic compounds dominated the
665 majority of detected species by FIGAERO-I-CIMS, in which CHO and CHON
666 compounds both accounted for significant fractions. Nitrogen-containing organic
667 compounds occupied a significant fraction of the total signals in both the gas and
668 particle phases, with elevated fractions at higher molecular weights. The most abundant
669 organic compounds were formic acid and multifunctional organic compounds
670 containing 3-5 oxygen atoms. Organic compounds containing 2-~~or~~-3 carbon atoms
671 accounted for over half of the total organic compounds in both gas- and particle-phase
672 measured by FIGAERO-I-CIMS. During the campaign, the FIGAERO-I-CIMS
673 measurements explained 24±0.8% of OA mass measured by AMS, but the fractions
674 ~~are~~ were higher for ~~measurements of~~ more aged organic aerosol ~~in the urban~~
675 ~~atmosphere.~~ This evidence, along with the analysis of the Van Krevelen plot,
676 ~~indicate~~ indicates that FIGAERO-I-CIMS ~~were~~ is measuring the more oxidized fraction
677 of OA in the urban air.

678 Our observations suggest that oxygenated organic compounds in urban
679 environments are complicated in both sources and chemistry. Oxygenated organic
680 compounds can be both emitted from various emission sources (e.g. vehicular
681 emissions and biomass burning) and also secondary produced in the atmosphere. The
682 chemistry in forming and removing these oxygenated organic compounds can be
683 associated with daytime and nocturnal reactions initiated from both anthropogenic and
684 biogenic precursors with strong influences from NO_x chemistry. This work
685 demonstrates that the rich information in both gas and particle phases provided by
686 FIGAERO-I-CIMS can greatly promote the understanding of emission and chemistry
687 of organic carbon in the atmosphere of urban regions.

688

689 **Acknowledgement**

690 This work was supported by the National Key R&D Plan of China (grant No.
691 2019YFE0106300, 2018YFC0213904, 2016YFC0202206), the National Natural
692 Science Foundation of China (grant No. 41877302), Guangdong Natural Science
693 Funds for Distinguished Young Scholar (grant No. 2018B030306037), Guangdong
694 Provincial Key R&D Plan (grant No. 2019B110206001), Guangdong Soft Science
695 Research Program (grant No. 2019B101001005) and Guangdong Innovative and
696 Entrepreneurial Research Team Program (grant No. 2016ZT06N263). This work was
697 also supported by Special Fund Project for Science and Technology Innovation Strategy
698 of Guangdong Province (Grant No.2019B121205004). Weiwei Hu and Wei Chen were
699 supported by National Natural Science Foundation of China (41875156).

700 **Data availability**

701 The more detailed data can be provided by contacting the corresponding authors.

702 **Author contributions**

703 BY and MS designed the research. CSY, YL, ZLW, TGL, WWH, WC, CHW,
704 CMW, SH, JPQ, BLW, CW, WS, XMW, ZYZ, XMW contributed to data collection.
705 CSY performed the data analysis with contributions from WWH and WC. CSY and
706 BY prepared the manuscript with contributions from JEK and other authors. All the
707 authors reviewed the manuscript.

708 **Competing interest**

709 The authors declare that they have no conflicts of interest.

710

711

712 **References**

713 Aiken, A. C., DeCarlo, P. F. and Jimenez, J. L.: Elemental Analysis of Organic
714 Species with Electron Ionization High-Resolution Mass Spectrometry, *Anal. Chem.*,
715 79(21), 8350–8358, doi:10.1021/ac071150w, 2007.

716 Aljawhary, D., Lee, A. K. Y. and Abbatt, J. P. D.: High-resolution chemical
717 ionization mass spectrometry (ToF-CIMS): Application to study SOA composition
718 and processing, *Atmos. Meas. Tech.*, 6(11), 3211–3224, doi:10.5194/amt-6-3211-
719 2013, 2013.

720 Bean, J. K. and Hildebrandt Ruiz, L.: Gas-particle partitioning and hydrolysis of
721 organic nitrates formed from the oxidation of alpha-pinene in environmental chamber
722 experiments, *Atmos. Chem. Phys.*, 16(4), 2175–2184, doi:10.5194/acp-16-2175-2016,
723 2016.

724 Berndt, T., Scholz, W., Mentler, B., Fischer, L., Herrmann, H., Kulmala, M. and
725 Hansel, A.: Accretion Product Formation from Self- and Cross-Reactions of RO₂
726 Radicals in the Atmosphere, *Angew. Chemie Int. Ed.*, 57(14), 3820–3824,
727 doi:10.1002/anie.201710989, 2018.

728 Berndt, T., Hyttinen, N., Herrmann, H. and Hansel, A.: First oxidation products from
729 the reaction of hydroxyl radicals with isoprene for pristine environmental conditions,
730 *Commun. Chem.*, 2(1), 1–10, doi:10.1038/s42004-019-0120-9, 2019.

731 Bertram, T. H., Thornton, J. A. and Riedel, T. P.: An experimental technique for the
732 direct measurement of N₂O₅ reactivity on ambient particles, *Atmos. Meas. Tech.*,
733 2(1), 231–242, doi:10.5194/amt-2-231-2009, 2009.

734 Bertram, T. H., Kimmel, J. R., Crisp, T. A., Ryder, O. S., Yatavelli, R. L. N.,
735 Thornton, J. A., Cubison, M. J., Gonin, M. and Worsnop, D. R.: A field-deployable,
736 chemical ionization time-of-flight mass spectrometer, *Atmos. Meas. Tech.*, 4(7),
737 1471–1479, doi:10.5194/amt-4-1471-2011, 2011.

738 Bhattarai, H., Saikawa, E., Wan, X., Zhu, H., Ram, K., Gao, S., Kang, S., Zhang, Q.,
739 Zhang, Y., Wu, G., Wang, X., Kawamura, K., Fu, P. and Cong, Z.: Levoglucosan as a
740 tracer of biomass burning: Recent progress and perspectives, *Atmos. Res.*,
741 220(November 2018), 20–33, doi:10.1016/j.atmosres.2019.01.004, 2019.

742 Boyd, C. M., Sanchez, J., Xu, L., Eugene, A. J., Nah, T., Tuet, W. Y., Guzman, M. I.
743 and Ng, N. L.: Secondary organic aerosol formation from the β -pinene+NO₃ system:
744 effect of humidity and peroxy radical fate, *Atmos. Chem. Phys.*, 15(13), 7497–7522,
745 doi:10.5194/acp-15-7497-2015, 2015.

746 Brandt, C. and van Eldik, R.: Transition Metal-Catalyzed Oxidation of Sulfur(IV)
747 Oxides. Atmospheric-Relevant Processes and Mechanisms, *Chem. Rev.*, 95(1), 119–
748 190, doi:10.1021/cr00033a006, 1995.

749 Brege, M., Paglione, M., Gilardoni, S., Decesari, S., Cristina Facchini, M. and
750 Mazzoleni, L. R.: Molecular insights on aging and aqueous-phase processing from
751 ambient biomass burning emissions-influenced Po Valley fog and aerosol, *Atmos.*
752 *Chem. Phys.*, 18(17), 13197–13214, doi:10.5194/acp-18-13197-2018, 2018.

753 Le Breton, M., Hallquist, A. M., Pathak, R. K., Simpson, D., Wang, Y., Johansson, J.,
754 Zheng, J., Yang, Y., Shang, D., Wang, H., Liu, Q., Chan, C., Wang, T., Bannan, T. J.,
755 Priestley, M., Percival, C. J., Shallcross, D. E., Lu, K., Guo, S., Hu, M. and Hallquist,
756 M.: Chlorine oxidation of VOCs at a semi-rural site in Beijing: significant chlorine
757 liberation from ClNO₂ and subsequent gas- and particle-phase Cl-VOC production,
758 *Atmos. Chem. Phys.*, 18(17), 13013–13030, doi:10.5194/acp-18-13013-2018, 2018a.

759 Le Breton, M., Wang, Y., Hallquist, Å. M., Pathak, R. K., Zheng, J., Yang, Y., Shang,
760 D., Glasius, M., Bannan, T. J., Liu, Q., Chan, C. K., Percival, C. J., Zhu, W., Lou, S.,
761 Topping, D., Wang, Y., Yu, J., Lu, K., Guo, S., Hu, M. and Hallquist, M.: Online gas-
762 and particle-phase measurements of organosulfates, organosulfonates and nitrooxy
763 organosulfates in Beijing utilizing a FIGAERO ToF-CIMS, *Atmos. Chem. Phys.*,
764 18(14), 10355–10371, doi:10.5194/acp-18-10355-2018, 2018b.

765 Le Breton, M., Psichoudaki, M., Hallquist, M., Watne, Å. K., Lutz, A. and Hallquist,
766 Å. M.: Application of a FIGAERO ToF CIMS for on-line characterization of real-
767 world fresh and aged particle emissions from buses, *Aerosol Sci. Technol.*, 53(3),
768 244–259, doi:10.1080/02786826.2019.1566592, 2019.

769 Canagaratna, M. R., Jimenez, J. L., Kroll, J. H., Chen, Q., Kessler, S. H., Massoli, P.
770 and Ruiz, L. H.: Elemental ratio measurements of organic compounds using aerosol
771 mass spectrometry: characterization, improved calibration, and implications, *Atmos.*
772 *Chem. Phys.*, 15, 253–272, doi:10.5194/acp-15-253-2015, 2015.

773 Capouet, M. and Müller, J. F.: A group contribution method for estimating the vapour
774 pressures of α -pinene oxidation products, *Atmos. Chem. Phys.*, 6(6), 1455–1467,
775 doi:10.5194/acp-6-1455-2006, 2006.

776 Carlton, A. G., Turpin, B. J., Altieri, K. E., Seitzinger, S., Reff, A., Lim, H.-J. and
777 Ervens, B.: Atmospheric oxalic acid and SOA production from glyoxal: Results of
778 aqueous photooxidation experiments, *Atmos. Environ.*, 41(35), 7588–7602,
779 doi:10.1016/j.atmosenv.2007.05.035, 2007.

780 Carslaw, N.: A mechanistic study of limonene oxidation products and pathways
781 following cleaning activities, *Atmos. Environ.*, 80, 507–513,
782 doi:https://doi.org/10.1016/j.atmosenv.2013.08.034, 2013.

783 Chen, H. and Finlayson-Pitts, B. J.: New Particle Formation from Methanesulfonic
784 Acid and Amines/Ammonia as a Function of Temperature, *Environ. Sci. Technol.*,
785 51(1), 243–252, doi:10.1021/acs.est.6b04173, 2017.

786 Chen, J., Wenger, J. C. and Venables, D. S.: Near-Ultraviolet Absorption Cross
787 Sections of Nitrophenols and Their Potential Influence on Tropospheric Oxidation
788 Capacity, *J. Phys. Chem. A*, 115(44), 12235–12242, doi:10.1021/jp206929r, 2011.

789 Cubison, M. J., Ortega, A. M., Hayes, P. L., Farmer, D. K., Day, D., Lechner, M. J.,
790 Brune, W. H., Apel, E., Diskin, G. S., Fisher, J. A., Fuelberg, H. E., Hecobian, A.,
791 Knapp, D. J., Mikoviny, T., Riemer, D., Sachse, G. W., Sessions, W., Weber, R. J.,
792 Weinheimer, A. J., Wisthaler, A. and Jimenez, J. L.: Effects of aging on organic
793 aerosol from open biomass burning smoke in aircraft and laboratory studies, *Atmos.*
794 *Chem. Phys.*, 11(23), 12049–12064, doi:10.5194/acp-11-12049-2011, 2011.

795 D’Ambro, E. L., Lee, B. H., Liu, J., Shilling, J. E., Gaston, C. J., Lopez-Hilfiker, F.
796 D., Schobesberger, S., Zaveri, R. A., Mohr, C., Lutz, A., Zhang, Z., Gold, A., Surratt,
797 J. D., Rivera-Rios, J. C., Keutsch, F. N. and Thornton, J. A.: Molecular composition
798 and volatility of isoprene photochemical oxidation secondary organic aerosol under
799 low- and high-NO_x conditions, *Atmos. Chem. Phys.*, 17(1), 159–174,
800 doi:10.5194/acp-17-159-2017, 2017.

801 D’Ambro, E. L., Schobesberger, S., Zaveri, R. A., Shilling, J. E., Lee, B. H., Lopez-
802 Hilfiker, F. D., Mohr, C. and Thornton, J.: Isothermal evaporation of α -pinene
803 ozonolysis SOA: volatility, phase state, and oligomeric composition, *ACS Earth Sp.*
804 *Chem.*, acsearthspacechem.8b00084, doi:10.1021/acsearthspacechem.8b00084, 2018.

805 Edwards, P. M., Brown, S. S., Roberts, J. M., Ahmadov, R., Banta, R. M., DeGouw,

806 J. A., Dubé, W. P., Field, R. A., Flynn, J. H., Gilman, J. B., Graus, M., Helmig, D.,
807 Koss, A., Langford, A. O., Lefer, B. L., Lerner, B. M., Li, R., Li, S. M., McKeen, S.
808 A., Murphy, S. M., Parrish, D. D., Senff, C. J., Soltis, J., Stutz, J., Sweeney, C.,
809 Thompson, C. R., Trainer, M. K., Tsai, C., Veres, P. R., Washenfelder, R. A.,
810 Warneke, C., Wild, R. J., Young, C. J., Yuan, B. and Zamora, R.: High winter ozone
811 pollution from carbonyl photolysis in an oil and gas basin, *Nature*, 514(7522), 351–
812 354, doi:10.1038/nature13767, 2014.

813 Eger, P. G., Schuladen, J., Sobanski, N., Fischer, H., Karu, E., Williams, J., Riva, M.,
814 Zha, Q., Ehn, M., Quéléver, L. L. J., Schallhart, S., Lelieveld, J. and Crowley, J. N.:
815 Pyruvic acid in the boreal forest: gas-phase mixing ratios and impact on radical
816 chemistry, *Atmos. Chem. Phys.*, 20(6), 3697–3711, doi:10.5194/acp-20-3697-2020,
817 2020.

818 Eisele, F. L. and Tanner, D. J.: Measurement of the gas phase concentration of
819 H₂SO₄ and methane sulfonic acid and estimates of H₂SO₄ production and loss in the
820 atmosphere, *J. Geophys. Res. Atmos.*, 98(D5), 9001–9010, doi:10.1029/93JD00031,
821 1993.

822 Fang, W., Gong, L. and Sheng, L.: Online analysis of secondary organic aerosols
823 from OH-initiated photooxidation and ozonolysis of α -pinene, β -pinene, Δ^3 -carene
824 and d-limonene by thermal desorption-photoionisation aerosol mass spectrometry,
825 *Environ. Chem.*, 14(2), 75–90, doi:10.1071/EN16128, 2017.

826 Faxon, C., Hammes, J., Pathak, R. K. and Hallquist, M.: Characterization of organic
827 nitrate constituents of secondary organic aerosol (SOA) from nitrate-radical-initiated
828 oxidation of limonene using High-Resolution Chemical Ionization Mass
829 Spectrometry, *Atmos. Chem. Phys.*, 18, 5467–5481, doi:10.5194/acp-2017-584, 2018.

830 Fisher, J. A., Jacob, D. J., Travis, K. R., Kim, P. S., Marais, E. A., Chan Miller, C.,
831 Yu, K., Zhu, L., Yantosca, R. M. and Sulprizio, M. P.: Organic Nitrate Chemistry and
832 its Implications for Nitrogen Budgets in an Isoprene- and Monoterpene-Rich
833 Atmosphere: Constraints from Aircraft (SEAC4RS) and Ground-Based (SOAS)
834 Observations in the Southeast US, *Atmos. Chem. Phys.*, 16, 5969 [online] Available
835 from: <https://www.atmos-chem-phys.net/16/5969/2016/acp-16-5969-2016.pdf>, 2016.

836 Fountoukis, C. and Nenes, A.: ISORROPIA II: a computationally efficient
837 thermodynamic equilibrium model for K^+ – Ca^{2+} – Mg^{2+} – NH_4^+ – Na^+ – SO_4^{2-} – NO_3^- –
838 Cl^- – H_2O aerosols, *Atmos. Chem. Phys.*, 7(17), 4639–4659, doi:10.5194/acp-7-
839 4639-2007, 2007.

840 Fry, J. L., Draper, D. C., Zarzana, K. J., Campuzano-Jost, P., Day, D. A., Jimenez, J.
841 L., Brown, S. S., Cohen, R. C., Kaser, L., Hansel, A., Cappellin, L., Karl, T., Hodzic
842 Roux, A., Turnipseed, A., Cantrell, C., Lefer, B. L., Grossberg, N., Farmer, D. K. and
843 Jimenez, J. L.: Observations of gas- and aerosol-phase organic nitrates at BEACHON-
844 RoMBAS 2011, *Atmos. Chem. Phys.*, 13(17), 8585–8605, doi:10.5194/acp-13-8585-
845 2013, 2013.

846 Galloway, M. M., Chhabra, P. S., Chan, A. W. H., Surratt, J. D., Flagan, R. C.,
847 Seinfeld, J. H. and Keutsch, F. N.: Glyoxal uptake on ammonium sulphate seed
848 aerosol: reaction products and reversibility of uptake under dark and irradiated
849 conditions, *Atmos. Chem. Phys.*, 9(10), 3331–3345, doi:10.5194/acp-9-3331-2009,
850 2009.

851 Gaston, C. J., Lopez-Hilfiker, F. D., Whybrew, L. E., Hadley, O., McNair, F., Gao,
852 H., Jaffe, D. A. and Thornton, J. A.: Online molecular characterization of fine
853 particulate matter in Port Angeles, WA: Evidence for a major impact from residential
854 wood smoke, *Atmos. Environ.*, 138, 99–107, doi:10.1016/j.atmosenv.2016.05.013,
855 2016.

856 Glasius, M., Lahaniati, M., Calogirou, A., Di Bella, D., Jensen, N. R., Hjorth, J.,
857 Kotzias, D. and Larsen, B. R.: Carboxylic acids in secondary aerosols from oxidation
858 of cyclic monoterpenes by ozone, *Environ. Sci. Technol.*, 34(6), 1001–1010,
859 doi:10.1021/es990445r, 2000.

860 Gondwe, M., Krol, M., Gieskes, W., Klaassen, W. and de Baar, H.: The contribution
861 of ocean-leaving DMS to the global atmospheric burdens of DMS, MSA, SO_2 , and
862 $NSS\ SO_4^{2-}$, *Global Biogeochem. Cycles*, 17(2), doi:10.1029/2002GB001937, 2003.

863 de Gouw, J. A., Middlebrook, A. M., Warneke, C., Goldan, P. D., Kuster, W. C.,
864 Roberts, J. M., Fehsenfeld, F. C., Worsnop, D. R., Canagaratna, M. R., Pszenny, A.
865 A. P., Keene, W. C., Marchewka, M., Bertman, S. B. and Bates, T. S.: Budget of

866 organic carbon in a polluted atmosphere: Results from the New England Air Quality
867 Study in 2002, *J. Geophys. Res. D Atmos.*, 110(16), 1–22,
868 doi:10.1029/2004JD005623, 2005.

869 de Gouw, J. A., Gilman, J. B., Kim, S. W., Alvarez, S. L., Dusanter, S., Graus, M.,
870 Griffith, S. M., Isaacman-VanWertz, G., Kuster, W. C., Lefer, B. L., Lerner, B. M.,
871 McDonald, B. C., Rappenglück, B., Roberts, J. M., Stevens, P. S., Stutz, J., Thalman,
872 R., Veres, P. R., Volkamer, R., Warneke, C., Washenfelder, R. A. and Young, C. J.:
873 Chemistry of Volatile Organic Compounds in the Los Angeles Basin: Formation of
874 Oxygenated Compounds and Determination of Emission Ratios, *J. Geophys. Res.*
875 *Atmos.*, 123(4), 2298–2319, doi:10.1002/2017JD027976, 2018.

876 Guo, H., Xu, L., Bougiatioti, A., Cerully, K. M., Capps, S. L., Hite, J. R., Carlton, A.
877 G., Lee, S. H., Bergin, M. H., Ng, N. L., Nenes, A. and Weber, R. J.: Fine-particle
878 water and pH in the southeastern United States, *Atmos. Chem. Phys.*, 15(9), 5211–
879 5228, doi:10.5194/acp-15-5211-2015, 2015.

880 Hallquist, M., Wenger, J. C., Baltensperger, U., Rudich, Y., Simpson, D., Claeys, M.,
881 Dommen, J., Donahue, N. M., George, C., Goldstein, a. H., Hamilton, J. F.,
882 Herrmann, H., Hoffmann, T., Iinuma, Y., Jang, M., Jenkin, M. E., Jimenez, J. L.,
883 Kiendler-Scharr, a., Maenhaut, W., McFiggans, G., Mentel, T. F., Monod, a.,
884 Prévôt, a. S. H., Seinfeld, J. H., Surratt, J. D., Szmigielski, R. and Wildt, J.: The
885 formation, properties and impact of secondary organic aerosol: current and emerging
886 issues, *Atmos. Chem. Phys.*, 9(14), 5155–5236, doi:10.5194/acp-9-5155-2009, 2009.

887 Hammes, J., Lutz, A., Mentel, T., Faxon, C. and Hallquist, M.: Carboxylic acids from
888 limonene oxidation by ozone and hydroxyl radicals: insights into mechanisms derived
889 using a FIGAERO-CIMS, *Atmos. Chem. Phys.*, 19(20), 13037–13052,
890 doi:10.5194/acp-19-13037-2019, 2019.

891 Harrison, M. A. J., Barra, S., Borghesi, D., Vione, D., Arsene, C. and Iulian Olariu,
892 R.: Nitrated phenols in the atmosphere: a review, *Atmos. Environ.*, 39(2), 231–248,
893 doi:https://doi.org/10.1016/j.atmosenv.2004.09.044, 2005.

894 He, Q.-F., Ding, X., Wang, X.-M., Yu, J.-Z., Fu, X.-X., Liu, T.-Y., Zhang, Z., Xue, J.,
895 Chen, D.-H., Zhong, L.-J. and Donahue, N. M.: Organosulfates from Pinene and

896 Isoprene over the Pearl River Delta, South China: Seasonal Variation and Implication
897 in Formation Mechanisms, *Environ. Sci. Technol.*, 48(16), 9236–9245,
898 doi:10.1021/es501299v, 2014.

899 Heald, C. L., Kroll, J. H., Jimenez, J. L., Docherty, K. S., Decarlo, P. F., Aiken, A. C.,
900 Chen, Q., Martin, S. T., Farmer, D. K. and Artaxo, P.: A simplified description of the
901 evolution of organic aerosol composition in the atmosphere, *Geophys. Res. Lett.*,
902 37(8), doi:10.1029/2010GL042737, 2010.

903 Hodzic, A., Jimenez, J. L., Madronich, S., Canagaratna, M. R., Decarlo, P. F.,
904 Kleinman, L. and Fast, J.: Modeling organic aerosols in a megacity: Potential
905 contribution of semi-volatile and intermediate volatility primary organic compounds
906 to secondary organic aerosol formation, *Atmos. Chem. Phys.*, 10(12), 5491–5514,
907 doi:10.5194/acp-10-5491-2010, 2010.

908 Hu, W., Hu, M., Hu, W., Jimenez, J. L., Yuan, B., Chen, W., Wang, M., Wu, Y.,
909 Chen, C., Wang, Z., Peng, J., Zeng, L. and Shao, M.: Chemical composition, sources,
910 and aging process of submicron aerosols in Beijing: Contrast between summer and
911 winter, *J. Geophys. Res. Atmos.*, 121(4), 1955–1977,
912 doi:10.1002/2015JD024020.Received, 2016.

913 Hu, W., Day, D. A., Campuzano-Jost, P., Nault, B. A., Park, T., Lee, T., Croteau, P.,
914 Canagaratna, M. R., Jayne, J. T., Worsnop, D. R. and Jimenez, J. L.: Evaluation of the
915 new capture vaporizer for aerosol mass spectrometers: Characterization of organic
916 aerosol mass spectra, *Aerosol Sci. Technol.*, 52(7), 725–739,
917 doi:10.1080/02786826.2018.1454584, 2018.

918 Huang, R.-J., Cao, J., Chen, Y., Yang, L., Shen, J., You, Q., Wang, K., Lin, C., Xu,
919 W., Gao, B., Li, Y., Chen, Q., Hoffmann, T., O’Dowd, C. D., Bilde, M. and Glasius,
920 M.: Organosulfates in atmospheric aerosol: synthesis and quantitative analysis of
921 PM_{2.5} from Xi’an, northwestern China, *Atmos. Meas. Tech.*, 11(6), 3447–3456,
922 doi:10.5194/amt-11-3447-2018, 2018.

923 Huang, R. J., Zhang, Y., Bozzetti, C., Ho, K. F., Cao, J. J., Han, Y., Daellenbach, K.
924 R., Slowik, J. G., Platt, S. M., Canonaco, F., Zotter, P., Wolf, R., Pieber, S. M., Bruns,
925 E. A., Crippa, M., Ciarelli, G., Piazzalunga, A., Schwikowski, M., Abbaszade, G.,

926 Schnelle-Kreis, J., Zimmermann, R., An, Z., Szidat, S., Baltensperger, U., El Haddad,
927 I. and Prévôt, A. S. H.: High secondary aerosol contribution to particulate pollution
928 during haze events in China, *Nature*, 514(7521), 218–222, doi:10.1038/nature13774,
929 2015.

930 Huang, W., Saathoff, H., Shen, X., Ramisetty, R., Leisner, T. and Mohr, C.: Chemical
931 Characterization of Highly Functionalized Organonitrates Contributing to Night-Time
932 Organic Aerosol Mass Loadings and Particle Growth, *Environ. Sci. Technol.*, 53(3),
933 1165–1174, doi:10.1021/acs.est.8b05826, 2019.

934 Hunter, J. F., Day, D. A., Palm, B. B., Yatavelli, R. L. N., Chan, A. W. H., Kaser, L.,
935 Cappellin, L., Hayes, P. L., Cross, E. S., Carrasquillo, A. J., Campuzano-Jost, P.,
936 Stark, H., Zhao, Y., Hohaus, T., Smith, J. N., Hansel, A., Karl, T., Goldstein, A. H.,
937 Guenther, A., Worsnop, D. R., Thornton, J. A., Heald, C. L., Jimenez, J. L. and Kroll,
938 J. H.: Comprehensive characterization of atmospheric organic carbon at a forested
939 site, *Nat. Geosci.*, 10(10), 748–753, doi:10.1038/NGEO3018, 2017.

940 Hyttinen, N., Otkjær, R. V., Iyer, S., Kjaergaard, H. G., Rissanen, M. P., Wennberg,
941 P. O. and Kurtén, T.: Computational Comparison of Different Reagent Ions in the
942 Chemical Ionization of Oxidized Multifunctional Compounds, *J. Phys. Chem. A*,
943 122(1), 269–279, doi:10.1021/acs.jpca.7b10015, 2018.

944 Isaacman-VanWertz, G., Massoli, P., O’Brien, R., Lim, C., Franklin, J., Moss, J.,
945 Hunter, J., Nowak, J., Canagaratna, M., Misztal, P., Arata, C., Roscioli, J., Herndon,
946 S., Onasch, T., Lambe, A., Jayne, J., Su, L., Knopf, D., Goldstein, A., Worsnop, D.
947 and Kroll, J.: Chemical evolution of atmospheric organic carbon over multiple
948 generations of oxidation, *Nat. Chem.*, 10(4), 462–468, doi:10.1038/s41557-018-0002-
949 2, 2018.

950 Iyer, S., Lopez-Hilfiker, F., Lee, B. H., Thornton, J. A. and Kurtén, T.: Modeling the
951 Detection of Organic and Inorganic Compounds Using Iodide-Based Chemical
952 Ionization, *J. Phys. Chem. A*, 120(4), 576–587, doi:10.1021/acs.jpca.5b09837, 2016.

953 Jacobs, M. I., Burke, W. J. and Elrod, M. J.: Kinetics of the Reactions of Isoprene-
954 Derived Hydroxynitrates: Gas Phase Epoxide Formation and Solution Phase
955 Hydrolysis, *Atmos. Chem. Phys.*, 14, 8933, 2014.

956 Jenkin, M. E., Saunders, S. M., Wagner, V. and Pilling, M. J.: Protocol for the
957 development of the Master Chemical Mechanism, MCM v3 (Part B): tropospheric
958 degradation of aromatic volatile organic compounds, *Atmos. Chem. Phys.*, 3(1), 181–
959 193, doi:10.5194/acp-3-181-2003, 2003.

960 Karl, T., Striednig, M., Graus, M., Hammerle, A. and Wohlfahrt, G.: Urban flux
961 measurements reveal a large pool of oxygenated volatile organic compound
962 emissions, *Proc. Natl. Acad. Sci.*, 201714715, doi:10.1073/pnas.1714715115, 2018.

963 Kawamura, K. and Bikkina, S.: A review of dicarboxylic acids and related
964 compounds in atmospheric aerosols: Molecular distributions, sources and
965 transformation, *Atmos. Res.*, 170, 140–160,
966 doi:https://doi.org/10.1016/j.atmosres.2015.11.018, 2016.

967 Kawamura, K., Kasukabe, H. and Barrie, L. A.: Source and reaction pathways of
968 dicarboxylic acids, ketoacids and dicarbonyls in arctic aerosols: One year of
969 observations, *Atmos. Environ.*, 30(10), 1709–1722, doi:https://doi.org/10.1016/1352-
970 2310(95)00395-9, 1996.

971 Kong, X., Salvador, C. M., Carlsson, S., Pathak, R., Davidsson, K. O., Le Breton, M.,
972 Gaita, S. M., Mitra, K., Hallquist, Å. M., Hallquist, M. and Pettersson, J. B. C.:
973 Molecular characterization and optical properties of primary emissions from a
974 residential wood burning boiler, *Sci. Total Environ.*, 754, 142143,
975 doi:https://doi.org/10.1016/j.scitotenv.2020.142143, 2021.

976 Krechmer, J. E., Pagonis, D., Ziemann, P. J. and Jimenez, J. L.: Quantification of Gas-
977 Wall Partitioning in Teflon Environmental Chambers Using Rapid Bursts of Low-
978 Volatility Oxidized Species Generated in Situ, *Environ. Sci. Technol.*, 50(11), 5757–
979 5765, doi:10.1021/acs.est.6b00606, 2016.

980 Kroll, J. H. and Seinfeld, J. H.: Chemistry of secondary organic aerosol: Formation
981 and evolution of low-volatility organics in the atmosphere, *Atmos. Environ.*, 42(16),
982 3593–3624, doi:10.1016/j.atmosenv.2008.01.003, 2008.

983 Lambe, A. T., Onasch, T. B., Croasdale, D. R., Wright, J. P., Martin, A. T., Franklin,
984 J. P., Massoli, P., Kroll, J. H., Canagaratna, M. R., Brune, W. H., Worsnop, D. R. and
985 Davidovits, P.: Transitions from functionalization to fragmentation reactions of

986 laboratory Secondary Organic Aerosol (SOA) generated from the OH oxidation of
987 alkane precursors, *Environ. Sci. Technol.*, 46(10), 5430–5437,
988 doi:10.1021/es300274t, 2012.

989 Larsen, B. R., Di Bella, D., Glasius, M., Winterhalter, R., Jensen, N. R. and Hjorth, J.:
990 Gas-phase OH oxidation of monoterpenes: Gaseous and particulate products, *J.*
991 *Atmos. Chem.*, 38(3), 231–276, doi:10.1023/A:1006487530903, 2001.

992 Lee, B. H., Lopez-Hilfiker, F. D., Mohr, C., Kurtén, T., Worsnop, D. R. and
993 Thornton, J. A.: An iodide-adduct high-resolution time-of-flight chemical-ionization
994 mass spectrometer: Application to atmospheric inorganic and organic compounds,
995 *Environ. Sci. Technol.*, 48(11), 6309–6317, doi:10.1021/es500362a, 2014.

996 Lee, B. H., Mohr, C., Lopez-Hilfiker, F. D., Lutz, A., Hallquist, M., Lee, L., Romer,
997 P., Cohen, R. C., Iyer, S., Kurtén, T., Hu, W., Day, D. A., Campuzano-Jost, P.,
998 Jimenez, J. L., Xu, L., Ng, N. L., Guo, H., Weber, R. J., Wild, R. J., Brown, S. S.,
999 Koss, A., de Gouw, J., Olson, K., Goldstein, A. H., Seco, R., Kim, S., McAvey, K.,
1000 Shepson, P. B., Starn, T., Baumann, K., Edgerton, E. S., Liu, J., Shilling, J. E., Miller,
1001 D. O., Brune, W., Schobesberger, S., D’Ambro, E. L. and Thornton, J. A.: Highly
1002 functionalized organic nitrates in the southeast United States: Contribution to
1003 secondary organic aerosol and reactive nitrogen budgets, *Proc. Natl. Acad. Sci.*,
1004 113(6), 1516–1521, doi:10.1073/pnas.1508108113, 2016.

1005 Lee, B. H., Lopez-hilfiker, F. D., Veres, P. R., Mcduffie, E. E., Fibiger, D. L.,
1006 Tamara, L. and Thornton, J. A.: Flight deployment of a high-resolution time-of-flight
1007 chemical ionization mass spectrometer : observations of reactive halogen and nitrogen
1008 oxide species, , doi:10.1029/2017JD028082, 2018a.

1009 Lee, B. H., Lopez-Hilfiker, F. D., D’Ambro, E. L., Zhou, P., Boy, M., Petäjä, T., Hao,
1010 L., Virtanen, A. and Thornton, J. A.: Semi-volatile and highly oxygenated gaseous
1011 and particulate organic compounds observed above a boreal forest canopy, *Atmos.*
1012 *Chem. Phys.*, 18(15), 11547–11562, doi:10.5194/acp-18-11547-2018, 2018b.

1013 Li, T., Wang, Z., Yuan, B., Ye, C., Lin, Y., Wang, S., Sha, Q., Yuan, Z., Zheng, J. and
1014 Shao, M.: Emissions of carboxylic acids, hydrogen cyanide (HCN) and isocyanic acid
1015 (HNCO) from vehicle exhaust, *Atmos. Environ.*, 247, 118218,

1016 doi:<https://doi.org/10.1016/j.atmosenv.2021.118218>, 2021.

1017 Liao, J., Froyd, K. D., Murphy, D. M., Keutsch, F. N., Yu, G., Wennberg, P. O., St
1018 Clair, J. M., Crouse, J. D., Wisthaler, A., Mikoviny, T., Jimenez, J. L., Campuzano-
1019 Jost, P., Day, D. A., Hu, W., Ryerson, T. B., Pollack, I. B., Peischl, J., Anderson, B.
1020 E., Ziemba, L. D., Blake, D. R., Meinardi, S. and Diskin, G.: Airborne measurements
1021 of organosulfates over the continental U.S, *J. Geophys. Res. Atmos.* JGR, 120(7),
1022 2990–3005, doi:10.1002/2014JD022378, 2015.

1023 Lim, H.-J., Carlton, A. G. and Turpin, B. J.: Isoprene Forms Secondary Organic
1024 Aerosol through Cloud Processing: Model Simulations, *Environ. Sci. Technol.*,
1025 39(12), 4441–4446, doi:10.1021/es048039h, 2005.

1026 Liu, C., Deng, X., Zhu, B. and Yin, C.: Characteristics of GSR of China’s three major
1027 economic regions in the past 10 years and its relationship with O₃ and PM_{2.5}, *China*
1028 *Environ. Sci.*, 38(08), 2820–2829, doi:10.19674/j.cnki.issn1000-6923.2018.0295,
1029 2018.

1030 Liu, X., Qu, H., Huey, L. G., Wang, Y., Sjostedt, S., Zeng, L., Lu, K., Wu, Y., Hu,
1031 M., Shao, M., Zhu, T. and Zhang, Y.: High Levels of Daytime Molecular Chlorine
1032 and Nitryl Chloride at a Rural Site on the North China Plain, *Environ. Sci. Technol.*,
1033 51(17), 9588–9595, doi:10.1021/acs.est.7b03039, 2017.

1034 Liu, Z., Wang, Y., Gu, D., Zhao, C., Huey, L. G., Stickel, R., Liao, J., Shao, M., Zhu,
1035 T., Zeng, L., Amoroso, A., Costabile, F., Chang, C. C. and Liu, S. C.: Summertime
1036 photochemistry during CAREBeijing-2007: RO_xbudgets and O₃ formation, *Atmos.*
1037 *Chem. Phys.*, 12(16), 7737–7752, doi:10.5194/acp-12-7737-2012, 2012.

1038 Lopez-Hilfiker, F. D., Mohr, C., Ehn, M., Rubach, F., Kleist, E., Wildt, J., Mentel, T.
1039 F., Lutz, A., Hallquist, M., Worsnop, D. and Thornton, J. A.: A novel method for
1040 online analysis of gas and particle composition: description and evaluation of a Filter
1041 Inlet for Gases and AEROSols (FIGAERO), *Atmos. Meas. Tech.*, 7(4), 983–1001,
1042 doi:10.5194/amt-7-983-2014, 2014.

1043 Lopez-Hilfiker, F. D., Mohr, C., Ehn, M., Rubach, F., Kleist, E., Wildt, J., Mentel, T.
1044 F. and Carrasquillo, A. J.: Phase partitioning and volatility of secondary organic
1045 aerosol components formed from α -pinene ozonolysis and OH oxidation : the

1046 importance of accretion products and other low volatility compounds, *Atmos. Chem.*
1047 *Phys.*, 15, 7765–7776, doi:10.5194/acp-15-7765-2015, 2015.

1048 Lopez-Hilfiker, F. D., Iyer, S., Mohr, C., Lee, B. H., Ambro, E. L. D., Kurtén, T. and
1049 Thornton, J. A.: Constraining the sensitivity of iodide adduct chemical ionization
1050 mass spectrometry to multifunctional organic molecules using the collision limit and
1051 thermodynamic stability of iodide ion adducts, *Atmos. Meas. Tech.*, 9, 1505–1512,
1052 doi:10.5194/amt-9-1505-2016, 2016.

1053 Massoli, P., Stark, H., Canagaratna, M. R., Krechmer, J. E., Xu, L., Ng, N. L.,
1054 Mauldin, R. L., Yan, C., Kimmel, J., Misztal, P. K., Jimenez, J. L., Jayne, J. T. and
1055 Worsnop, D. R.: Ambient Measurements of Highly Oxidized Gas-Phase Molecules
1056 during the Southern Oxidant and Aerosol Study (SOAS) 2013, *ACS Earth Sp. Chem.*,
1057 2(7), 653–672, doi:10.1021/acsearthspacechem.8b00028, 2018.

1058 Mattila, J. M., Brophy, P., Kirkland, J., Hall, S., Ullmann, K., Fischer, E. V., Brown,
1059 S., McDuffie, E., Tevlin, A. and Farmer, D. K.: Tropospheric sources and sinks of
1060 gas-phase acids in the Colorado Front Range, *Atmos. Chem. Phys.*, 18(16), 12315–
1061 12327, doi:10.5194/acp-18-12315-2018, 2018.

1062 Mehra, A., Wang, Y., Krechmer, J. E., Lambe, A., Majluf, F., Morris, M. A.,
1063 Priestley, M., Bannan, T. J., Bryant, D. J., Pereira, K. L., Hamilton, J. F., Rickard, A.
1064 R., Newland, M. J., Stark, H., Croteau, P., Jayne, J. T., Worsnop, D. R., Canagaratna,
1065 M. R., Wang, L. and Coe, H.: Evaluation of the chemical composition of gas- and
1066 particle-phase products of aromatic oxidation, *Atmos. Chem. Phys.*, 20(16), 9783–
1067 9803, doi:10.5194/acp-20-9783-2020, 2020.

1068 Mellouki, A., Wallington, T. J. and Chen, J.: Atmospheric Chemistry of Oxygenated
1069 Volatile Organic Compounds: Impacts on Air Quality and Climate, *Chem. Rev.*,
1070 115(10), 3984–4014, doi:10.1021/cr500549n, 2015.

1071 Mohr, C., Lopez-Hilfiker, F. D., Zotter, P., Prévôt, A. S. H., Xu, L., Ng, N. L.,
1072 Herndon, S. C., Williams, L. R., Franklin, J. P., Zahniser, M. S., Worsnop, D. R.,
1073 Knighton, W. B., Aiken, A. C., Gorkowski, K. J., Dubey, M. K., Allan, J. D. and
1074 Thornton, J. A.: Contribution of Nitrated Phenols to Wood Burning Brown Carbon
1075 Light Absorption in Detling, United Kingdom during Winter Time, *Environ. Sci.*

1076 Technol., 47(12), 6316–6324, doi:10.1021/es400683v, 2013.

1077 Mutzel, A., Poulain, L., Berndt, T., Iinuma, Y., Rodigast, M., Böge, O., Richters, S.,
1078 Spindler, G., Sipilä, M., Jokinen, T., Kulmala, M. and Herrmann, H.: Highly
1079 Oxidized Multifunctional Organic Compounds Observed in Tropospheric Particles: A
1080 Field and Laboratory Study, Environ. Sci. Technol., 49(13), 7754–7761,
1081 doi:10.1021/acs.est.5b00885, 2015.

1082 Mutzel, A., Rodigast, M., Iinuma, Y., Böge, O. and Herrmann, H.: Monoterpene SOA
1083 - Contribution of first-generation oxidation products to formation and chemical
1084 composition, Atmos. Environ., 130, 136–144, doi:10.1016/j.atmosenv.2015.10.080,
1085 2016.

1086 Nah, T., Sanchez, J., Boyd, C. M. and Ng, N. L.: Photochemical Aging of α -pinene
1087 and β -pinene Secondary Organic Aerosol formed from Nitrate Radical Oxidation,
1088 Environ. Sci. Technol., 50(1), 222–231, doi:10.1021/acs.est.5b04594, 2016.

1089 Nannoolal, Y., Rarey, J. and Ramjugernath, D.: Estimation of pure component
1090 properties Part 3. Estimation of the vapor pressure of non-electrolyte organic
1091 compounds via group contributions and group interactions, Fluid Phase Equilib.,
1092 269(1–2), 117–133, doi:10.1016/j.fluid.2008.04.020, 2008.

1093 Ng, N. L., Brown, S. S., Archibald, A. T., Atlas, E., Cohen, R. C., Crowley, J. N.,
1094 Day, D. A., Donahue, N. M., Fry, J. L., Fuchs, H., Griffin, R. J., Guzman, M. I.,
1095 Herrmann, H., Hodzic, A., Iinuma, Y., Jimenez, J. L., Kiendler-Scharr, A., Lee, B. H.,
1096 Luecken, D. J., Mao, J., McLaren, R., Mutzel, A., Osthoff, H. D., Ouyang, B.,
1097 Picquet-Varrault, B., Platt, U., Pye, H. O. T., Rudich, Y., Schwantes, R. H., Shiraiwa,
1098 M., Stutz, J., Thornton, J. A., Tilgner, A., Williams, B. J. and Zaveri, R. A.: Nitrate
1099 radicals and biogenic volatile organic compounds: oxidation, mechanisms, and
1100 organic aerosol, Atmos. Chem. Phys., 17(3), 2103–2162, doi:10.5194/acp-17-2103-
1101 2017, 2017.

1102 Noelscher, A. C., Yanez-Serrano, A. M., Wolff, S., de Araujo, A. C., Lavric, J. V,
1103 Kesselmeier, J. and Williams, J.: Unexpected seasonality in quantity and composition
1104 of Amazon rainforest air reactivity, Nat. Commun., 7, doi:10.1038/ncomms10383,
1105 2016.

1106 Osthoff, H. D., Roberts, J. M., Ravishankara, A. R., Williams, E. J., Lerner, B. M.,
1107 Sommariva, R., Bates, T. S., Coffman, D., Quinn, P. K., Dibb, J. E., Stark, H.,
1108 Burkholder, J. B., Talukdar, R. K., Meagher, J., Fehsenfeld, F. C. and Brown, S. S.:
1109 High levels of nitryl chloride in the polluted subtropical marine boundary layer, *Nat.*
1110 *Geosci.*, 1(5), 324–328, doi:10.1038/ngeo177, 2008.

1111 Palm, B. B., Liu, X., Jimenez, J. L. and Thornton, J. A.: Performance of a new coaxial
1112 ion-molecule reaction region for low-pressure chemical ionization mass spectrometry
1113 with reduced instrument wall interactions, *Atmos. Meas. Tech.*, 12(11), 5829–5844,
1114 doi:10.5194/amt-12-5829-2019, 2019.

1115 Pankow, J. F. and Asher, W. E.: SIMPOL.1: A simple group contribution method for
1116 predicting vapor pressures and enthalpies of vaporization of multifunctional organic
1117 compounds, *Atmos. Chem. Phys.*, 8(10), 2773–2796, doi:10.5194/acp-8-2773-2008,
1118 2008.

1119 Paulot, F., Crouse, J. D., Kjaergaard, H. G., Kroll, J. H., Seinfeld, J. H. and
1120 Wennberg, P. O.: Isoprene photooxidation: New insights into the production of acids
1121 and organic nitrates, *Atmos. Chem. Phys.*, 9(4), 1479–1501, doi:10.5194/acp-9-1479-
1122 2009, 2009.

1123 Qi, L., Chen, M., Stefenelli, G., Pospisilova, V., Tong, Y., Bertrand, A., Hueglin, C.,
1124 Ge, X., Baltensperger, U., Prévôt, A. S. H. and Slowik, J. G.: Organic aerosol source
1125 apportionment in Zurich using an extractive electrospray ionization time-of-flight
1126 mass spectrometer (EESI-TOF-MS) – Part 2: Biomass burning influences in winter,
1127 *Atmos. Chem. Phys.*, 19(12), 8037–8062, doi:10.5194/acp-19-8037-2019, 2019.

1128 Reyes-Villegas, E., Bannan, T., Le Breton, M., Mehra, A., Priestley, M., Percival, C.,
1129 Coe, H. and Allan, J. D.: Online Chemical Characterization of Food-Cooking Organic
1130 Aerosols: Implications for Source Apportionment, *Environ. Sci. Technol.*, 52(9),
1131 5308–5318, doi:10.1021/acs.est.7b06278, 2018.

1132 Riva, M., Rantala, P., Krechmer, J. E., Peräkylä, O., Zhang, Y., Heikkinen, L.,
1133 Garmash, O., Yan, C., Kulmala, M., Worsnop, D. and Ehn, M.: Evaluating the
1134 performance of five different chemical ionization techniques for detecting gaseous
1135 oxygenated organic species, *Atmos. Meas. Tech.*, 2018(4), 1–39, doi:10.5194/amt-

1136 2018-407, 2019.

1137 Sander, R. and Crutzen, P. J.: Model study indicating halogen activation and ozone
1138 destruction in polluted air masses transported to the sea, *J. Geophys. Res. Atmos.*,
1139 101(D4), 9121–9138, doi:10.1029/95JD03793, 1996.

1140 Schneider, J., Weimer, S., Drewnick, F., Borrmann, S., Helas, G., Gwaze, P., Schmid,
1141 O., Andreae, M. O. and Kirchner, U.: Mass spectrometric analysis and aerodynamic
1142 properties of various types of combustion-related aerosol particles, *Int. J. Mass*
1143 *Spectrom.*, 258(1), 37–49, doi:https://doi.org/10.1016/j.ijms.2006.07.008, 2006.

1144 Schwantes, R. H., Teng, A. P., Nguyen, T. B., Coggon, M. M., Crounse, J. D., St
1145 Clair, J. M., Zhang, X., Schilling, K. A., Seinfeld, J. H. and Wennberg, P. O.:
1146 Isoprene NO₃ Oxidation Products from the RO₂ + HO₂ Pathway, *J. Phys. Chem. A*,
1147 119, 10158, 2015.

1148 Schwantes, R. H., Schilling, K. A., McVay, R. C., Lignell, H., Coggon, M. M.,
1149 Zhang, X., Wennberg, P. O. and Seinfeld, J. H.: Formation of highly oxygenated low-
1150 volatility products from cresol oxidation, *Atmos. Chem. Phys.*, 17(5), 3453–3474,
1151 doi:10.5194/acp-17-3453-2017, 2017.

1152 Schwantes, R. H., Emmons, L. K., Orlando, J. J., Barth, M. C., Tyndall, G. S., Hall, S.
1153 R., Ullmann, K., St. Clair, J. M., Blake, D. R., Wisthaler, A. and Paul V. Bui, T.:
1154 Comprehensive isoprene and terpene gas-phase chemistry improves simulated surface
1155 ozone in the southeastern US, *Atmos. Chem. Phys.*, 20(6), 3739–3776,
1156 doi:10.5194/acp-20-3739-2020, 2020.

1157 Shrivastava, M., Andreae, M. O., Artaxo, P., Barbosa, H. M. J., Berg, L. K., Brito, J.,
1158 Ching, J., Easter, R. C., Fan, J., Fast, J. D., Feng, Z., Fuentes, J. D., Glasius, M.,
1159 Goldstein, A. H., Alves, E. G., Gomes, H., Gu, D., Guenther, A., Jathar, S. H., Kim,
1160 S., Liu, Y., Lou, S., Martin, S. T., McNeill, V. F., Medeiros, A., de Sá, S. S., Shilling,
1161 J. E., Springston, S. R., Souza, R. A. F., Thornton, J. A., Isaacman-VanWertz, G.,
1162 Yee, L. D., Ynoue, R., Zaveri, R. A., Zelenyuk, A. and Zhao, C.: Urban pollution
1163 greatly enhances formation of natural aerosols over the Amazon rainforest, *Nat.*
1164 *Commun.*, 10(1), doi:10.1038/s41467-019-08909-4, 2019.

1165 Simoneit, B. R. T., Schauer, J. J., Nolte, C. G., Oros, D. R., Elias, V. O., Fraser, M.

1166 P., Rogge, W. F. and Cass, G. R.: Levoglucosan, a tracer for cellulose in biomass
1167 burning and atmospheric particles, *Atmos. Environ.*, 33(2), 173–182,
1168 doi:[https://doi.org/10.1016/S1352-2310\(98\)00145-9](https://doi.org/10.1016/S1352-2310(98)00145-9), 1999.

1169 Slusher, D. L., Huey, L. G., Tanner, D. J., Flocke, F. M. and Roberts, J. M.: A thermal
1170 dissociation–chemical ionization mass spectrometry (TD-CIMS) technique for the
1171 simultaneous measurement of peroxyacyl nitrates and dinitrogen pentoxide, *J.*
1172 *Geophys. Res. Atmos.*, 109(D19), doi:10.1029/2004JD004670, 2004.

1173 Stark, H., Yatavelli, R. L. N., Thompson, S. L., Kimmel, J. R., Cubison, M. J.,
1174 Chhabra, P. S., Canagaratna, M. R., Jayne, J. T., Worsnop, D. R. and Jimenez, J. L.:
1175 Methods to extract molecular and bulk chemical information from series of complex
1176 mass spectra with limited mass resolution, *Int. J. Mass Spectrom.*, 389, 26–38,
1177 doi:10.1016/j.ijms.2015.08.011, 2015.

1178 Stark, H., Yatavelli, R. L. N., Thompson, S. L., Kang, H., Krechmer, J. E., Kimmel, J.
1179 R., Palm, B. B., Hu, W., Hayes, P. L., Day, D. A., Campuzano-Jost, P., Canagaratna,
1180 M. R., Jayne, J. T., Worsnop, D. R. and Jimenez, J. L.: Impact of Thermal
1181 Decomposition on Thermal Desorption Instruments: Advantage of Thermogram
1182 Analysis for Quantifying Volatility Distributions of Organic Species, *Environ. Sci.*
1183 *Technol.*, 51(15), 8491–8500, doi:10.1021/acs.est.7b00160, 2017.

1184 Stolzenburg, D., Fischer, L., Vogel, A. L., Heinritzi, M., Schervish, M., Simon, M.,
1185 Wagner, A. C., Dada, L., Ahonen, L. R., Amorim, A., Baccarini, A., Bauer, P. S.,
1186 Baumgartner, B., Bergen, A., Bianchi, F., Breitenlechner, M., Brilke, S., Buenrostro
1187 Mazon, S., Chen, D., Dias, A., Draper, D. C., Duplissy, J., El Haddad, I.,
1188 Finkenzeller, H., Frege, C., Fuchs, C., Garmash, O., Gordon, H., He, X., Helm, J.,
1189 Hofbauer, V., Hoyle, C. R., Kim, C., Kirkby, J., Kontkanen, J., Kürten, A.,
1190 Lampilahti, J., Lawler, M., Lehtipalo, K., Leiminger, M., Mai, H., Mathot, S.,
1191 Mentler, B., Molteni, U., Nie, W., Nieminen, T., Nowak, J. B., Ojdanic, A., Onnela,
1192 A., Passananti, M., Petäjä, T., Quéléver, L. L. J., Rissanen, M. P., Sarnela, N.,
1193 Schallhart, S., Tauber, C., Tomé, A., Wagner, R., Wang, M., Weitz, L., Wimmer, D.,
1194 Xiao, M., Yan, C., Ye, P., Zha, Q., Baltensperger, U., Curtius, J., Dommen, J., Flagan,
1195 R. C., Kulmala, M., Smith, J. N., Worsnop, D. R., Hansel, A., Donahue, N. M.,

1196 Winkler, P. M., Nie, W., Passananti, M., Leiminger, M., Stolzenburg, D., Yan, C.,
1197 Wimmer, D., Buenrostro Mazon, S., Kontkanen, J., Wang, M., Garmash, O., Kulmala,
1198 M., Petäjä, T., Bianchi, F., Chen, D., Nieminen, T., Brilke, S., Nowak, J. B., Duplissy,
1199 J., El Haddad, I., Simon, M., Wagner, A. C., Kürten, A., Smith, J. N., Kim, C., et al.:
1200 Rapid growth of organic aerosol nanoparticles over a wide tropospheric temperature
1201 range, *Proc. Natl. Acad. Sci.*, 115(37), 201807604, doi:10.1073/pnas.1807604115,
1202 2018.

1203 Surratt, J. D., Murphy, S. M., Kroll, J. H., Ng, N. L., Hildebrandt, L., Sorooshian, A.,
1204 Szmigielski, R., Vermeylen, R., Maenhaut, W., Claeys, M., Flagan, R. C. and
1205 Seinfeld, J. H.: Chemical Composition of Secondary Organic Aerosol Formed from
1206 the Photooxidation of Isoprene, *J. Phys. Chem. A*, 110(31), 9665–9690,
1207 doi:10.1021/jp061734m, 2006.

1208 Surratt, J. D., Kroll, J. H., Kleindienst, T. E., Edney, E. O., Claeys, M., Sorooshian,
1209 A., Ng, N. L., Offenberg, J. H., Lewandowski, M., Jaoui, M., Flagan, R. C. and
1210 Seinfeld, J. H.: Evidence for Organosulfates in Secondary Organic Aerosol, *Environ.*
1211 *Sci. Technol.*, 41(2), 517–527, doi:10.1021/es062081q, 2007.

1212 Surratt, J. D., Chan, A. W. H., Eddingsaas, N. C., Chan, M., Loza, C. L., Kwan, A. J.,
1213 Hersey, S. P., Flagan, R. C., Wennberg, P. O. and Seinfeld, J. H.: Reactive
1214 intermediates revealed in secondary organic aerosol formation from isoprene, *Proc.*
1215 *Natl. Acad. Sci.*, 107(15), 6640–6645, doi:10.1073/pnas.0911114107, 2010.

1216 Thornton, J. A., Mohr, C., Schobesberger, S., D’Ambro, E. L., Lee, B. H. and Lopez-
1217 Hilfiker, F. D.: Evaluating Organic Aerosol Sources and Evolution with a Combined
1218 Molecular Composition and Volatility Framework Using the Filter Inlet for Gases and
1219 Aerosols (FIGAERO), *Acc. Chem. Res.*, 53(8), 1415–1426,
1220 doi:10.1021/acs.accounts.0c00259, 2020.

1221 Volkamer, R., Jimenez, J. L., San Martini, F., Dzepina, K., Zhang, Q., Salcedo, D.,
1222 Molina, L. T., Worsnop, D. R. and Molina, M. J.: Secondary organic aerosol
1223 formation from anthropogenic air pollution: Rapid and higher than expected,
1224 *Geophys. Res. Lett.*, 33(17), doi:10.1029/2006GL026899, 2006.

1225 Wang, H., Gao, Y., Wang, S., Wu, X., Liu, Y., Li, X., Huang, D., Lou, S., Wu, Z.,

1226 Guo, S., Jing, S., Li, Y., Huang, C., Tyndall, G. S., Orlando, J. J. and Zhang, X.:
1227 Atmospheric Processing of Nitrophenols and Nitrocresols from Biomass Burning
1228 Emissions, *J. Geophys. Res. Atmos.*, 0–3, doi:10.1029/2020JD033401, 2020a.
1229 Wang, M., Chen, D., Xiao, M., Ye, Q., Stolzenburg, D., Hofbauer, V., Ye, P., Vogel,
1230 A. L., Mauldin, R. L., Amorim, A., Baccarini, A., Baumgartner, B., Brilke, S., Dada,
1231 L., Dias, A., Duplissy, J., Finkenzeller, H., Garmash, O., He, X.-C., Hoyle, C. R.,
1232 Kim, C., Kvashnin, A., Lehtipalo, K., Fischer, L., Molteni, U., Petäjä, T., Pospisilova,
1233 V., Quéléver, L. L. J., Rissanen, M., Simon, M., Tauber, C., Tomé, A., Wagner, A. C.,
1234 Weitz, L., Volkamer, R., Winkler, P. M., Kirkby, J., Worsnop, D. R., Kulmala, M.,
1235 Baltensperger, U., Dommen, J., El-Haddad, I. and Donahue, N. M.: Photo-oxidation
1236 of Aromatic Hydrocarbons Produces Low-Volatility Organic Compounds, *Environ.*
1237 *Sci. Technol.*, 54(13), 7911–7921, doi:10.1021/acs.est.0c02100, 2020b.
1238 Wang, Q., He, X., Zhou, M., Huang, D. D., Qiao, L., Zhu, S., Ma, Y., Wang, H., Li,
1239 L., Huang, C., Huang, X. H. H., Xu, W., Worsnop, D., Goldstein, A. H., Guo, H. and
1240 Yu, J. Z.: Hourly Measurements of Organic Molecular Markers in Urban Shanghai,
1241 China: Primary Organic Aerosol Source Identification and Observation of Cooking
1242 Aerosol Aging, *ACS Earth Sp. Chem.*, 4(9), 1670–1685,
1243 doi:10.1021/acsearthspacechem.0c00205, 2020c.
1244 Wang, T., Tham, Y. J., Xue, L., Li, Q., Zha, Q., Wang, Z., Poon, S. C. N., Dube, W.
1245 P., Blake, D. R., Louie, P. K. K., Luk, C. W. Y., Tsui, W., Brown, S. S., Osthoff, H.
1246 D., Roberts, J. M., Ravishankara, A. R., Williams, E. J., Lerner, B. M., Sommariva,
1247 R., Bates, T. S., Coffman, D., Quinn, P. K., Dibb, J. E., Stark, H., Burkholder, J. B.,
1248 Talukdar, R. K., Meagher, J., Fehsenfeld, F. C. and Brown, S. S.: Observations of
1249 nitryl chloride and modeling its source and effect on ozone in the planetary boundary
1250 layer of southern China, *J. Geophys. Res.*, 121(5), 2476–2489,
1251 doi:10.1002/2015JD024556, 2016.
1252 Wang, X., Jacob, D. J., Eastham, S. D., Sulprizio, M. P., Zhu, L., Chen, Q.,
1253 Alexander, B., Sherwen, T., Evans, M. J., Lee, B. H., Haskins, J. D., Lopez-Hilfiker,
1254 F. D., Thornton, J. A., Huey, G. L. and Liao, H.: The role of chlorine in global
1255 tropospheric chemistry, *Atmos. Chem. Phys.*, 19(6), 3981–4003, doi:10.5194/acp-19-

1256 3981-2019, 2019.

1257 Wang, Z., Yuan, B., Ye, C., Roberts, J., Wisthaler, A., Lin, Y., Li, T., Wu, C., Peng,
1258 Y., Wang, C., Wang, S., Yang, S., Wang, B., Qi, J., Wang, C., Song, W., Hu, W.,
1259 Wang, X., Xu, W., Ma, N., Kuang, Y., Tao, J., Zhang, Z., Su, H., Cheng, Y., Wang,
1260 X. and Shao, M.: High Concentrations of Atmospheric Isocyanic Acid (HNCO)
1261 Produced from Secondary Sources in China, *Environ. Sci. Technol.*, 11818–11826,
1262 doi:10.1021/acs.est.0c02843, 2020d.

1263 Wennberg, P. O., Bates, K. H., Crounse, J. D., Dodson, L. G., McVay, R. C., Mertens,
1264 L. A., Nguyen, T. B., Praske, E., Schwantes, R. H., Smarte, M. D., St Clair, J. M.,
1265 Teng, A. P., Zhang, X. and Seinfeld, J. H.: Gas-Phase Reactions of Isoprene and Its
1266 Major Oxidation Products, *Chem. Rev.*, 118(7), 3337–3390,
1267 doi:10.1021/acs.chemrev.7b00439, 2018.

1268 Wu, C., Wang, C., Wang, S., Wang, W., Yuan, B., Qi, J., Wang, B., Wang, H., Wang,
1269 C., Song, W., Wang, X., Hu, W., Lou, S., Ye, C., Peng, Y., Wang, Z., Huangfu, Y.,
1270 Xie, Y., Zhu, M., Zheng, J., Wang, X., Jiang, B., Zhang, Z. and Shao, M.:
1271 Measurement report: Important contributions of oxygenated compounds to emissions
1272 and chemistry of VOCs in urban air, *Atmos. Chem. Phys.*, 14769–14785,
1273 doi:10.5194/acp-2020-152, 2020.

1274 Xiong, F., McAvey, K. M., Pratt, K. A., Groff, C. J., Hostetler, M. A., Lipton, M. A.,
1275 Starn, T. K., Seeley, J. V, Bertman, S. B. and Teng, A. P.: Observation of Isoprene
1276 Hydroxynitrates in the Southeastern United States and Implications for the Fate of
1277 NO_x, *Atmos. Chem. Phys.*, 15, 11257, 2015.

1278 Xue, L., Gu, R., Wang, T., Wang, X., Saunders, S., Blake, D., Louie, P. K. K., Luk,
1279 C. W. Y., Simpson, I., Xu, Z., Wang, Z., Gao, Y., Lee, S., Mellouki, A. and Wang,
1280 W.: Oxidative capacity and radical chemistry in the polluted atmosphere of Hong
1281 Kong and Pearl River Delta region: analysis of a severe photochemical smog episode,
1282 *Atmos. Chem. Phys.*, 16(15), 9891–9903, doi:10.5194/acp-16-9891-2016, 2016.

1283 Yang, Y., Shao, M., Wang, X., Nölscher, A. C., Kessel, S., Guenther, A. and
1284 Williams, J.: Towards a quantitative understanding of total OH reactivity: A review,
1285 *Atmos. Environ.*, 134(2), 147–161, doi:10.1016/j.atmosenv.2016.03.010, 2016.

1286 Yang, Y., Shao, M., Keßel, S., Li, Y., Lu, K., Lu, S., Williams, J., Zhang, Y., Zeng,
1287 L., Nölscher, A. C., Wu, Y., Wang, X. and Zheng, J.: How the OH reactivity affects
1288 the ozone production efficiency: case studies in Beijing and Heshan, China, *Atmos.*
1289 *Chem. Phys.*, 17(11), 7127–7142, doi:10.5194/acp-17-7127-2017, 2017.

1290 Yasmeen, F., Szmigielski, R., Vermeylen, R., Gomez-Gonzalez, Y., Surratt, J. D.,
1291 Chan, A. W. H., Seinfeld, J. H., Maenhaut, W. and Claeys, M.: Mass spectrometric
1292 characterization of isomeric terpenoic acids from the oxidation of alpha-pinene, beta-
1293 pinene, d-limonene, and Delta(3)-carene in fine forest aerosol, *J. MASS Spectrom.*,
1294 46(4), 425–442, doi:10.1002/jms.1911, 2011.

1295 Yatavelli, R. L. N., Lopez-Hilfiker, F., Wargo, J. D., Kimmel, J. R., Cubison, M. J.,
1296 Bertram, T. H., Jimenez, J. L., Gonin, M., Worsnop, D. R. and Thornton, J. A.: A
1297 Chemical Ionization High-Resolution Time-of-Flight Mass Spectrometer Coupled to a
1298 Micro Orifice Volatilization Impactor (MOVI-HRToF-CIMS) for Analysis of Gas and
1299 Particle-Phase Organic Species, *Aerosol Sci. Technol.*, 46(12), 1313–1327,
1300 doi:10.1080/02786826.2012.712236, 2012.

1301 Yuan, B., Veres, P. R., Warneke, C., Roberts, J. M., Gilman, J. B., Koss, A., Edwards,
1302 P. M., Graus, M., Kuster, W. C., Li, S. M., Wild, R. J., Brown, S. S., Dubé, W. P.,
1303 Lerner, B. M., Williams, E. J., Johnson, J. E., Quinn, P. K., Bates, T. S., Lefter, B.,
1304 Hayes, P. L., Jimenez, J. L., Weber, R. J., Zamora, R., Ervens, B., Millet, D. B.,
1305 Rappenglück, B. and De Gouw, J. A.: Investigation of secondary formation of formic
1306 acid: Urban environment vs. oil and gas producing region, *Atmos. Chem. Phys.*,
1307 15(4), 1975–1993, doi:10.5194/acp-15-1975-2015, 2015.

1308 Yuan, B., Liggio, J., Wentzell, J., Li, S. M., Stark, H., Roberts, J. M., Gilman, J.,
1309 Lerner, B., Warneke, C., Li, R., Leithead, A., Osthoff, H. D., Wild, R., Brown, S. S.
1310 and De Gouw, J. A.: Secondary formation of nitrated phenols: Insights from
1311 observations during the Uintah Basin Winter Ozone Study (UBWOS) 2014, *Atmos.*
1312 *Chem. Phys.*, 16(4), 2139–2153, doi:10.5194/acp-16-2139-2016, 2016.

1313 Yuan, B., Koss, A. R., Warneke, C., Coggon, M., Sekimoto, K. and De Gouw, J. A.:
1314 Proton-Transfer-Reaction Mass Spectrometry: Applications in Atmospheric Sciences,
1315 *Chem. Rev.*, 117(21), 13187–13229, doi:10.1021/acs.chemrev.7b00325, 2017.

1316 Zhang, Q., Yuan, B., Shao, M., Wang, X., Lu, S., Lu, K., Wang, M., Chen, L., Chang,
1317 C.-C. and Liu, S. C.: Variations of ground-level O₃ and its precursors in Beijing in
1318 summertime between 2005 and 2011, *Atmos. Chem. Phys.*, 14(12), 6089–6101,
1319 doi:10.5194/acp-14-6089-2014, 2014.

1320 Zhang, Y. J., Tang, L. L., Wang, Z., Yu, H. X., Sun, Y. L., Liu, D., Qin, W.,
1321 Canonaco, F., Prévôt, A. S. H., Zhang, H. L. and Zhou, H. C.: Insights into
1322 characteristics, sources, and evolution of submicron aerosols during harvest seasons in
1323 the Yangtze River delta region, China, *Atmos. Chem. Phys.*, 15(3), 1331–1349,
1324 doi:10.5194/acp-15-1331-2015, 2015.

1325 Zhao, R.: *The Recent Development and Application of Chemical Ionization Mass*
1326 *Spectrometry in Atmospheric Chemistry.*, 2018.

1327 Zhao, Y., Nguyen, N. T., Presto, A. A., Hennigan, C. J., May, A. A. and Robinson, A.
1328 L.: Intermediate Volatility Organic Compound Emissions from On-Road Gasoline
1329 Vehicles and Small Off-Road Gasoline Engines, *Environ. Sci. Technol.*, 50(8), 4554–
1330 4563, doi:10.1021/acs.est.5b06247, 2016.

1331 Zhou, Y., Huang, X. H., Bian, Q., Griffith, S. M., Louie, P. K. K. and Yu, J. Z.:
1332 Sources and atmospheric processes impacting oxalate at a suburban coastal site in
1333 Hong Kong: Insights inferred from 1 year hourly measurements, *J. Geophys. Res.*
1334 *Atmos.*, 120(18), 9772–9788, doi:10.1002/2015JD023531, 2015.

1335

1336 **Table 1.** The detected ions discussed in the text.

Ion formula	m/z	Assigned compounds	Possible formation pathways	References
$C_6H_{10}O_5I^-$	288.96	Levoglucosan, mannosan and galactosan	Biomass burning or cooking emissions	(Gaston et al., 2016; Reyes-Villegas et al., 2018)
$C_6H_{12}O_5I^-$	290.97	Fucose	Biomass burning emissions	(Qi et al., 2019)
$C_6H_5NO_3I^-$	265.93	Nitro-phenols	Direct emissions, oxidation of aromatics in the presence of NO _x	(Gaston et al., 2016; Yuan et al., 2016)
$C_6H_5NO_4I^-$	281.93	Nitro-benzenediols	Direct emissions, oxidation of aromatics in the presence of NO _x	(Gaston et al., 2016; Yuan et al., 2016)
$C_6H_4N_2O_5I^-$	310.92	Dinitro-phenols	Direct emissions, oxidation of aromatics in the presence of NO _x	(Gaston et al., 2016; Yuan et al., 2016)
$C_7H_7NO_3I^-$	279.95	Methyl nitro-phenols	Direct emissions, oxidation of aromatics in the presence of NO _x	(Gaston et al., 2016; Yuan et al., 2016)
$C_7H_7NO_4I^-$	295.94	Methyl nitro-benzenediols	Direct emissions, oxidation of aromatics in the presence of NO _x	(Gaston et al., 2016; Yuan et al., 2016)
$C_7H_6O_4I^-$	280.93	Dihydroxy methyl benzoquinone	Aromatics + OH	(Schwantes et al., 2017; Wang et al., 2020b)
$C_7H_8O_4I^-$	282.95	Tetrahydroxy toluene	Aromatics + OH	(Schwantes et al., 2017; Wang et al., 2020b)
$C_7H_8O_5I^-$	298.94	Pentahydroxy toluene, fragments of C9 aromatics	Aromatics + OH	(Mehra et al., 2020; Schwantes et al., 2017)

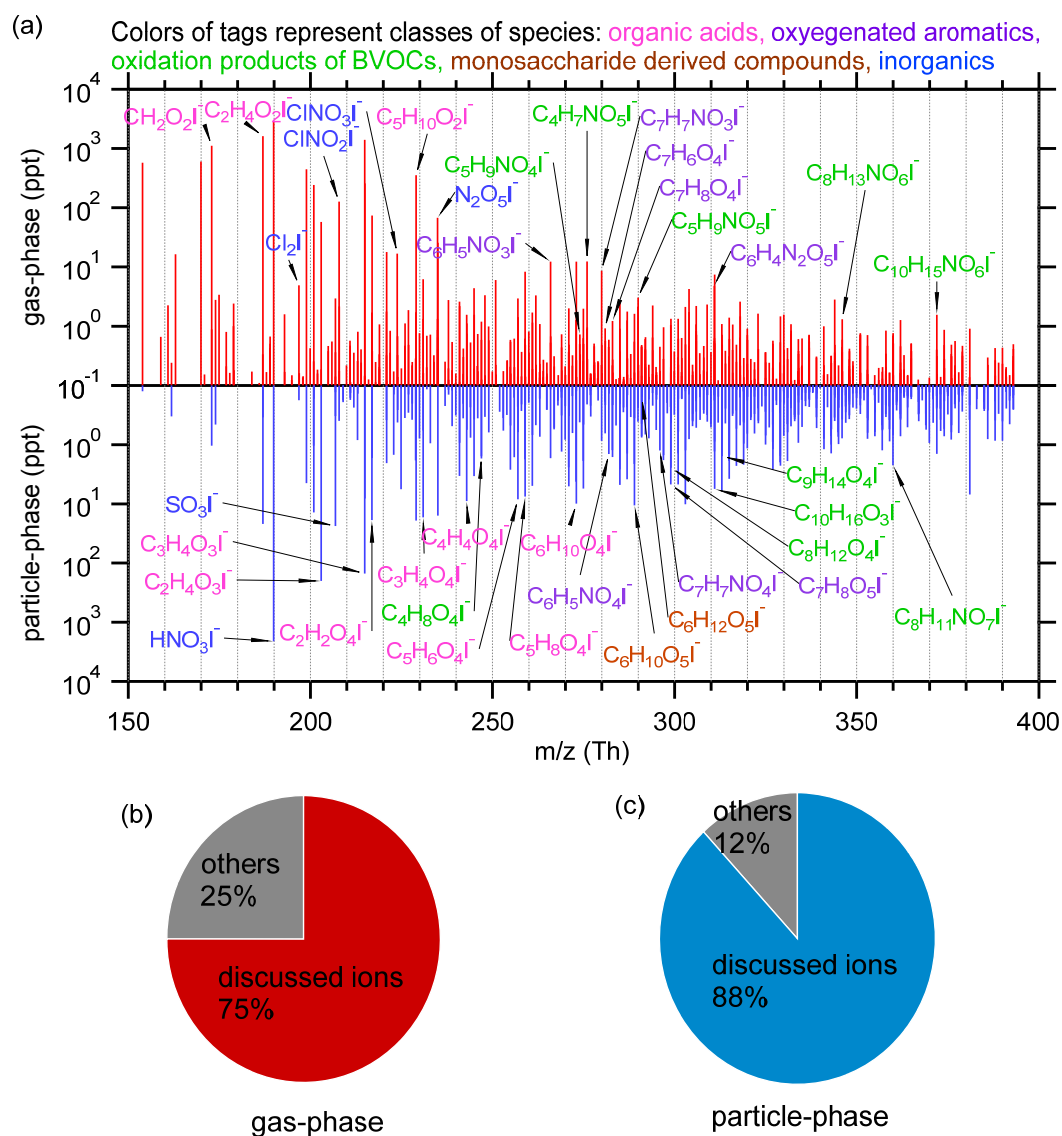
$CH_2O_2I^-$	172.91	Formic acid	Oxidation of VOCs	(Lee et al., 2014; Yuan et al., 2015)
$C_2H_4O_2I^-$	186.93	Acetic acid	Oxidation of VOCs	(Lee et al., 2014; Mattila et al., 2018)
$C_5H_{10}O_2I^-$	228.97	Pentanoic acid	Traffic emissions, secondary formation	(Mattila et al., 2018)
$C_2H_4O_3I^-$	202.92	Glycolic acid	Oxidation of VOCs	(Lee et al., 2014; Lim et al., 2005)
$C_3H_4O_3I^-$	214.92	Pyruvic acid	Photolysis of methylglyoxal, BVOCs+OH, photo- oxidation of aromatics in the presence of NO _x	(Eger et al., 2020; Mattila et al., 2018)
$C_2H_2O_4I^-$	216.90	Oxalic acid	Aqueous-phase photooxidation of glyoxal, photo-oxidation of VOCs	(Carlton et al., 2007; Lee et al., 2014; Zhou et al., 2015)
$C_3H_4O_4I^-$	230.92	Malonic acid, hydroxypyruvic acid	Oxidation of VOCs	(Kawamura and Bikkina, 2016; Lee et al., 2014)
$C_4H_4O_4I^-$	242.92	Maleic acid, fumaric acid	Oxidation of aromatics	(Brege et al., 2018; Kawamura et al., 1996)
$C_5H_6O_4I^-$	256.93	Unsaturated dicarboxylic acid	Oxidation of aromatics	(Brege et al., 2018; Kawamura et al., 1996)
$C_5H_8O_4I^-$	258.95		Photo-oxidation of VOCs	(Berndt et al., 2019; Kawamura and Bikkina, 2016)
$C_6H_{10}O_4I^-$	272.96		Photo-oxidation of VOCs	(Berndt et al., 2019; Kawamura and Bikkina, 2016)

$C_4H_8O_4I^-$	246.95	2-methylglyceric acid	Isoprene SOA component under high NO _x conditions	(Surratt et al., 2006, 2010)
$C_5H_9NO_4I^-$	273.96	IHN (isoprene hydroxy nitrates)	1st-generation organic nitrates from reaction: isoprene+OH+NO _x , isoprene+NO ₃	(Jacobs et al., 2014; Xiong et al., 2015)
$C_4H_7NO_5I^-$	275.94	MVKN/MACRN	2nd-generation organic nitrates from oxidation of IHN in the presence of NO _x	(Fisher et al., 2016; Paulot et al., 2009)
$C_5H_9NO_5I^-$	289.95	C5 nitrooxy hydroperoxide, C5 nitrooxy hydroxyepoxide, C5 dihydroxy nitrate	isoprene+NO ₃ , isoprene+OH+NO _x	(Ng et al., 2017; Schwantes et al., 2015; Wennberg et al., 2018)
$C_8H_{12}O_4I^-$	298.98	Dicarboxylic and oxocarboxylic acids like norpinic acid, terpenylic acid	Monoterpenes+OH, monoterpenes O ₃	(Fang et al., 2017; Mutzel et al., 2016; Yasmeen et al., 2011)
$C_9H_{14}O_4I^-$	312.99	Dicarboxylic and oxocarboxylic acids like pinic acid, homoterpenylic acid, caric acid	Monoterpenes+OH, monoterpenes O ₃	(Fang et al., 2017; Mutzel et al., 2016; Yasmeen et al., 2011)
$C_{10}H_{16}O_3I^-$	311.02	Oxocarboxylic acids like	Monoterpenes+OH, monoterpenes O ₃	(Fang et al., 2017; Glasius et al.,

		pinonic acid, caronic acid		2000; Yasmeen et al., 2011)
$C_8H_{13}NO_6I^-$	345.98	Organic nitrates from monoterpenes	Monoterpenes+OH+NO _x , monoterpenes +NO ₃	(Lee et al., 2016; Nah et al., 2016)
$C_8H_{11}NO_7I^-$	359.96	Organic nitrates from monoterpenes	Monoterpenes+OH+NO _x , monoterpenes O ₃ +NO ₃	(Carslaw, 2013; Lee et al., 2016)
$C_{10}H_{15}NO_6I^-$	372.00	Organic nitrates from monoterpenes, peroxyacetyl nitrate from pinonaldehyde	Monoterpenes+OH+NO _x , monoterpenes O ₃ +NO ₃	(Boyd et al., 2015; Massoli et al., 2018; Schwantes et al., 2020)
HSO_4^-	96.96	Sulfuric acid	Oxidation of SO ₂ etc.	(Le Breton et al., 2018b)
SO_3I^-	206.86	Sulfur trioxide, Fragment of organosulfates	Oxidation of SO ₂ , decomposition of organosulfates	(Surratt et al., 2007)
$C_2H_3SO_6^-$	154.96	Glycolic acid sulfate	Aqueous reaction of glycolic acid and sulfuric acid	(Galloway et al., 2009; Huang et al., 2018)
$CH_3SO_3^-$	94.98	Methanesulfonic acid	Oxidation of dimethyl sulfide	(Chen and Finlayson-Pitts, 2017; Gondwe et al., 2003)
$N_2O_5I^-$	234.89	Dinitrogen pentoxide	NO ₃ + NO ₂ + M	(Le Breton et al., 2018a; Wang et al., 2016)
$ClNO_2I^-$	207.87	Nitryl chloride	N ₂ O ₅ (g) + Cl ⁻ (aq)	(Le Breton et al., 2018a; Wang et al., 2016)

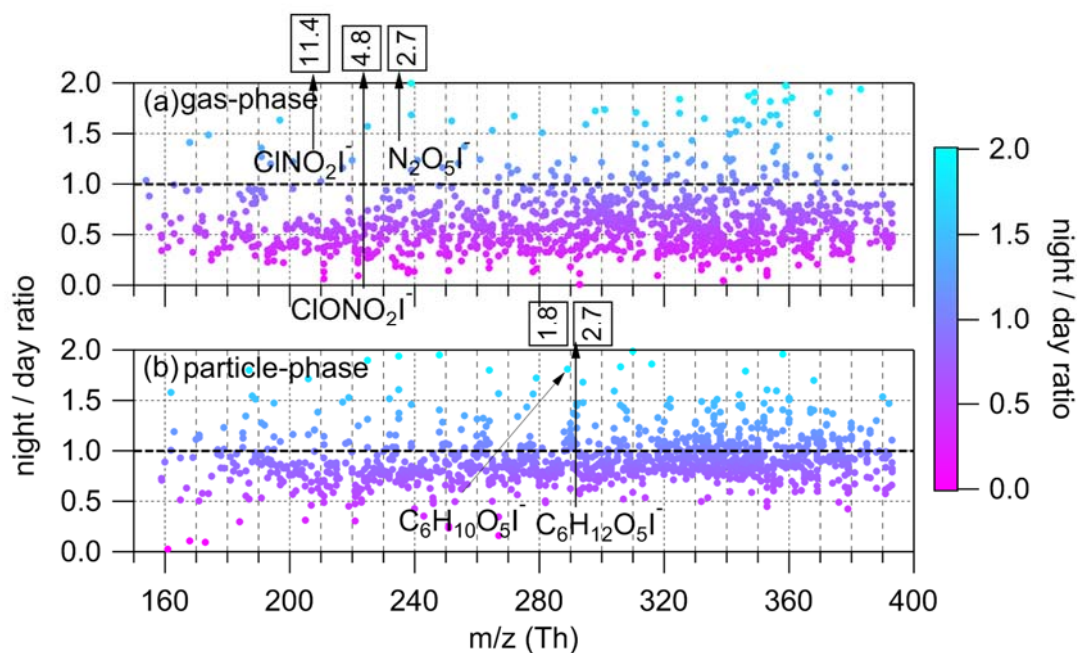
$ClNO_3I^-$	223.86	Chlorine nitrate	$ClO + NO_2 + M$	(Liu et al., 2017; Sander and Crutzen, 1996)
Cl_2I^-	196.84	Chlorine	Heterogeneous reactions of Cl^- and reactive chlorine like HOCl, $ClNO_2$ etc.	(Le Breton et al., 2018a; Liu et al., 2017; Wang et al., 2019)
HNO_3I^-	189.90	Nitric acid	$NO_x + OH$, hydrolysis of organic nitrates and N_2O_5	(Fisher et al., 2016; Wang et al., 2016)

1337



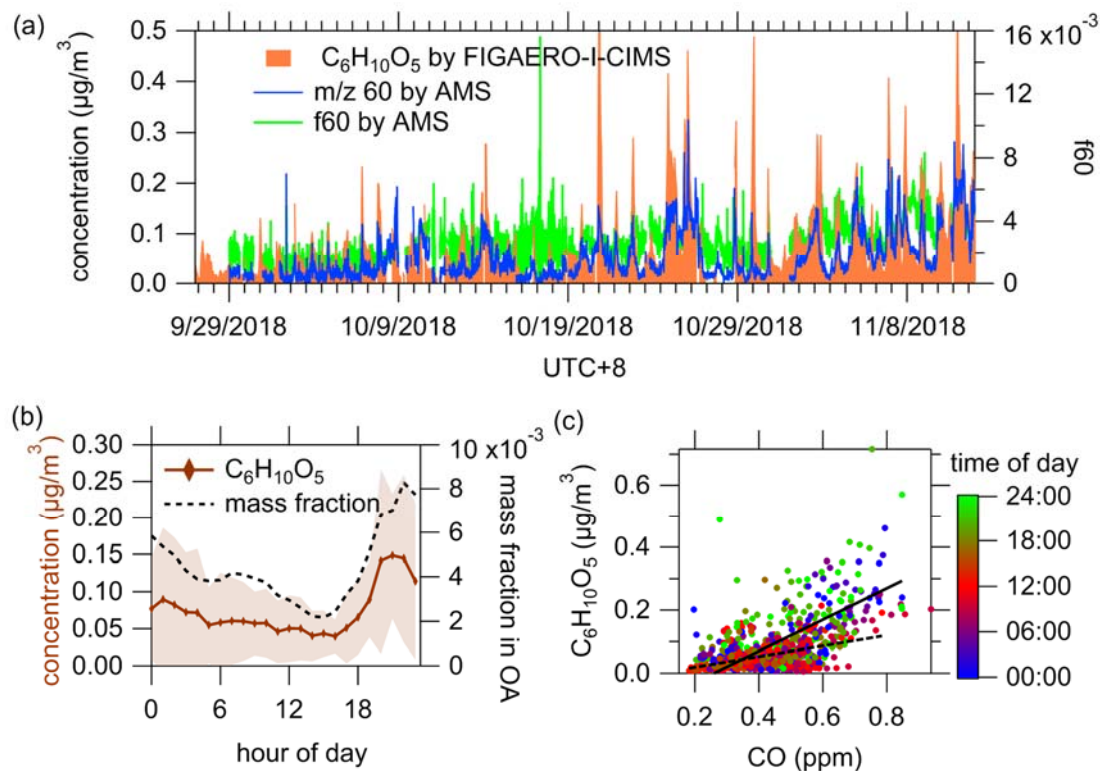
1339

1340 **Figure 1.** (a) Mass spectra of iodide charged ion within m/z 150-400 Th in gas-phase
 1341 (red) and particle-phase (blue), respectively. (b and c) The fractions of I-adduct ions
 1342 discussed in the main text (Table 1) in the total ion signals for I-adduct ions measured
 1343 in gas-phase (b) and particle-phase (c), respectively.



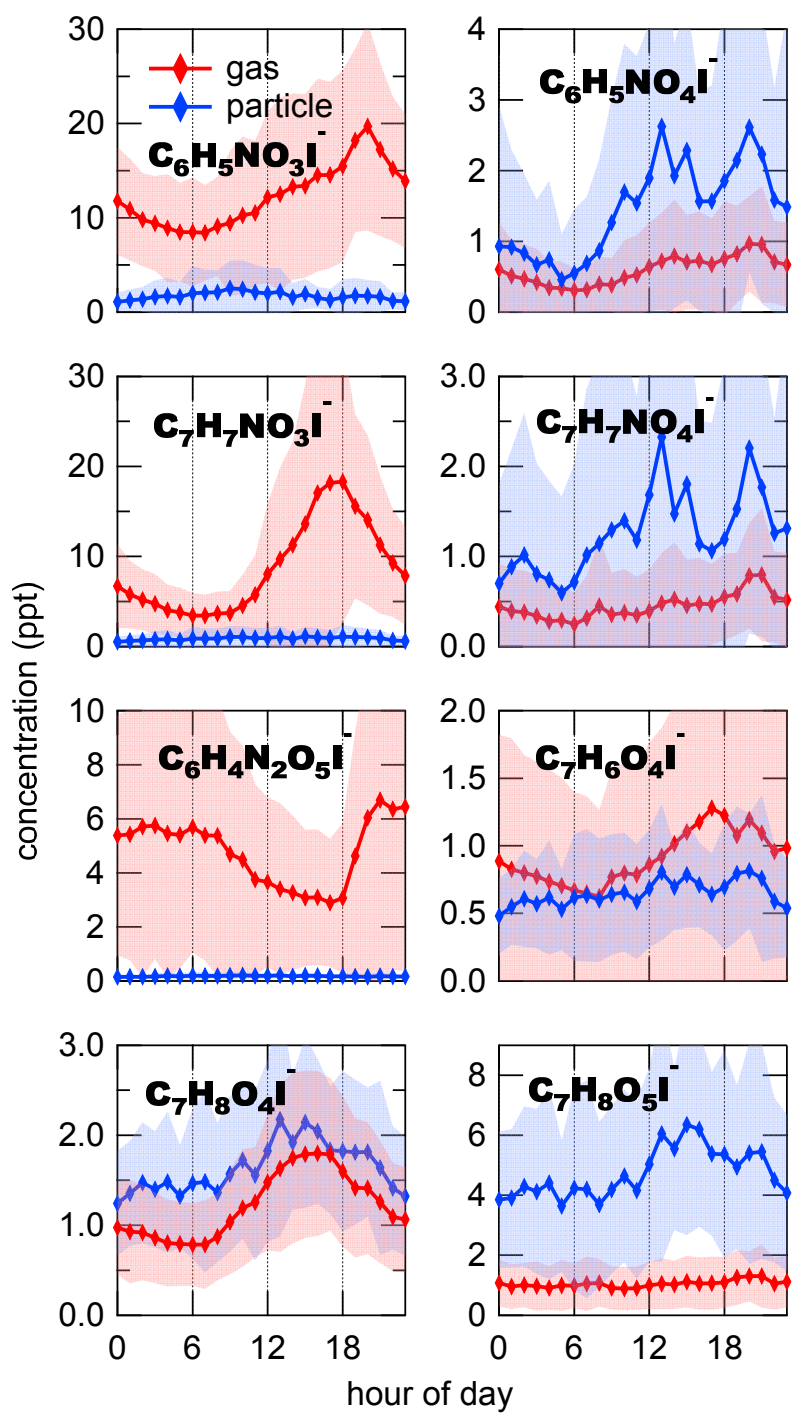
1345

1346 **Figure 2.** The ratios of concentrations at night (10 pm - 6 am) to concentrations during
 1347 the day (10 am - 6 pm) for ions ranging from 150 to 400 Th in gas-phase (a) and particle-
 1348 phase (b). The range of y-axis is set between 0 and 2 for clarity, although the ratios of
 1349 some compounds are larger than 2. The numbers in boxes indicate the night/day ratios
 1350 of tagged ions that exceed the y-axis ranges.



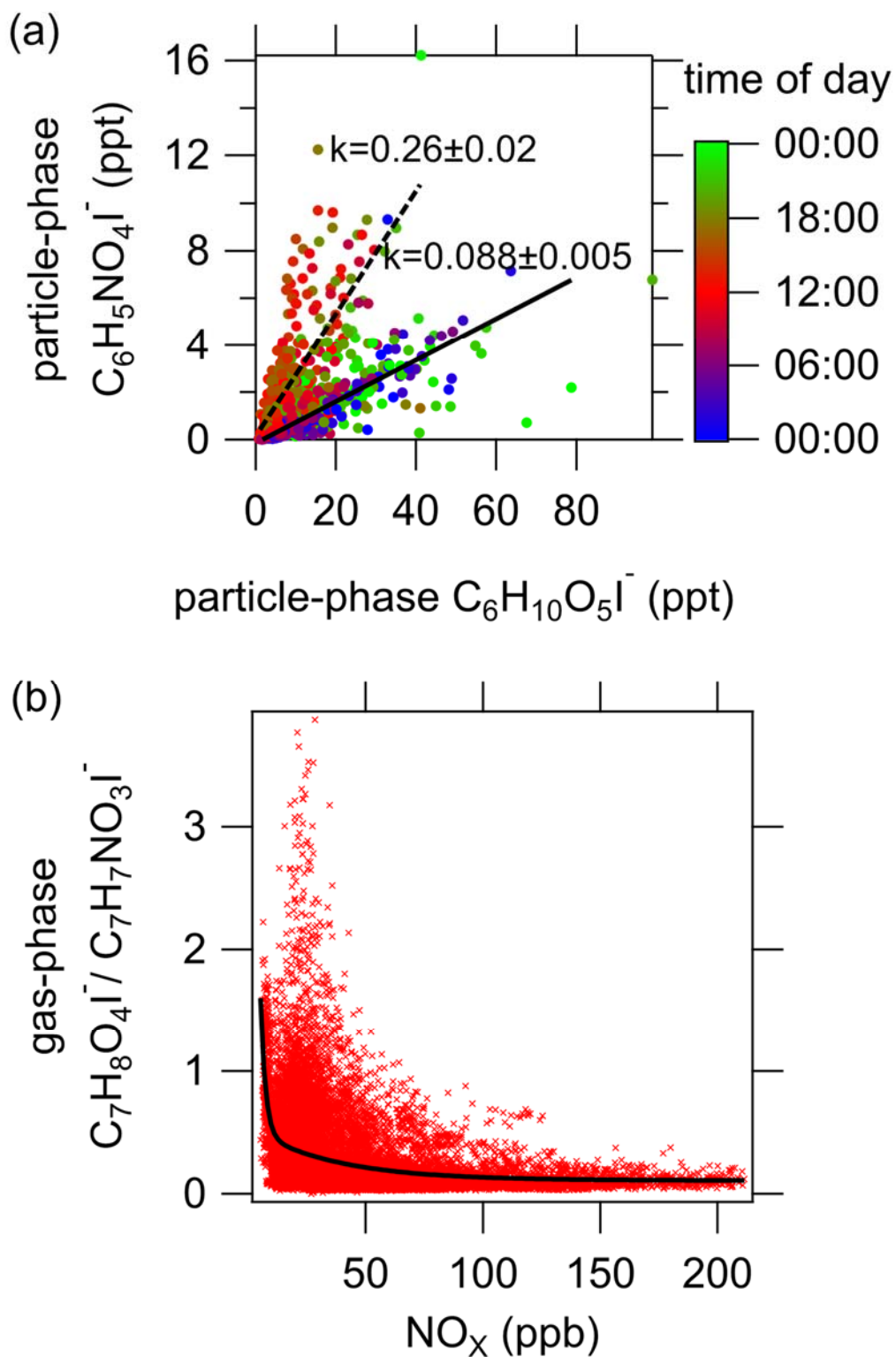
1351

1352 **Figure 3.** (a) Time series of particulate $\text{C}_6\text{H}_{10}\text{O}_5$ measured by FIGAERO-I-CIMS, m/z
 1353 60 fragment and $\text{f}60$ measured by AMS. Background $\text{f}60=0.3\%$ and background m/z
 1354 $60=0.3\% \times \text{OA}$ were subtracted from $\text{f}60$ and m/z 60 (Cubison et al., 2011; Hu et al.,
 1355 2016). (b) Diurnal variations of particulate $\text{C}_6\text{H}_{10}\text{O}_5$ and its mass fraction in OA. (c)
 1356 Correlation between CO and particulate $\text{C}_6\text{H}_{10}\text{O}_5$. The dash and solid lines indicate the
 1357 ratios during daytime (10 am - 6 pm, $0.17 \pm 0.02 \mu\text{g} \cdot \text{m}^{-3}/\text{ppm}$) and nighttime (10 pm - 6
 1358 am, $0.50 \pm 0.03 \mu\text{g} \cdot \text{m}^{-3}/\text{ppm}$), respectively.



1359

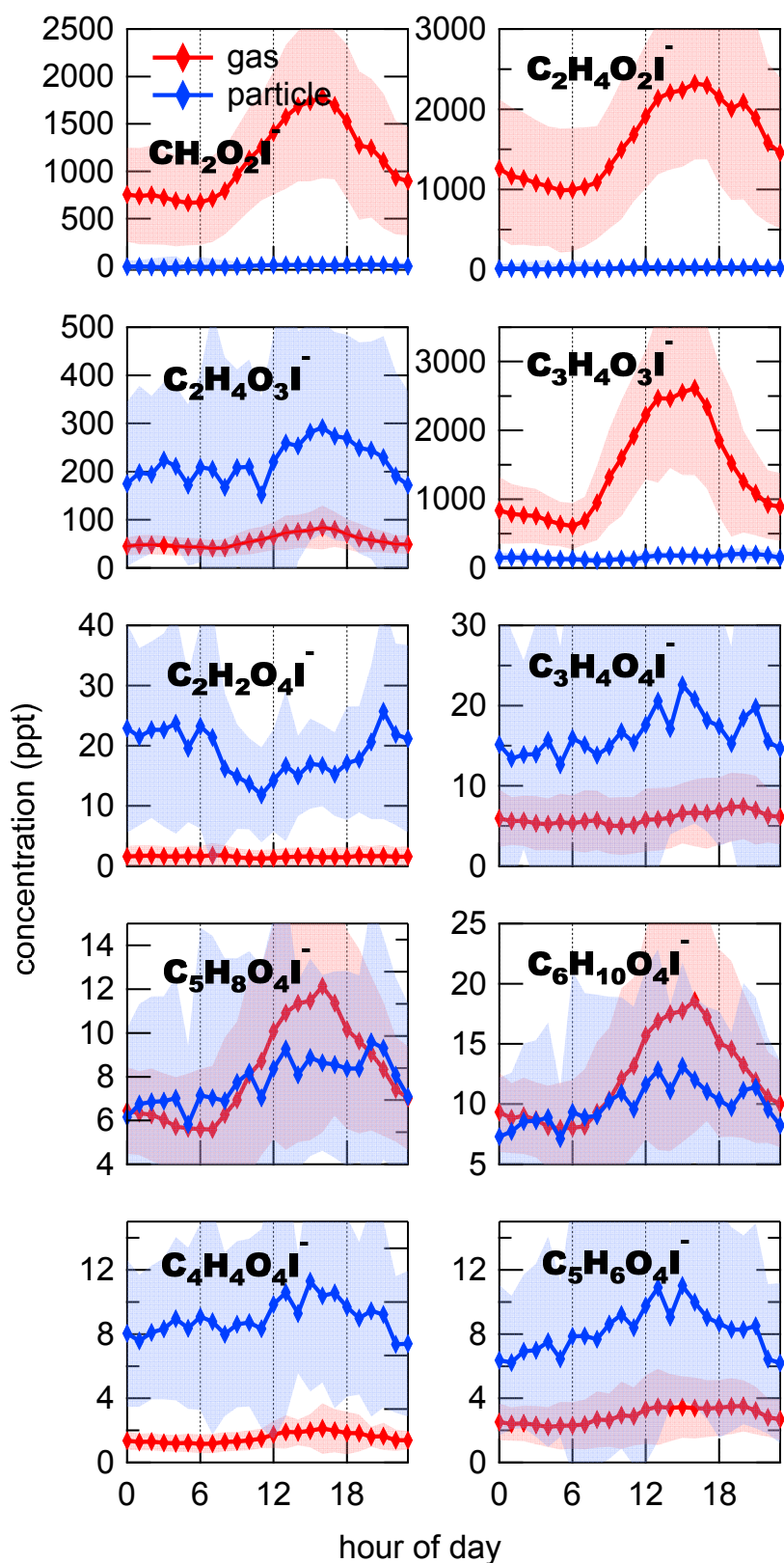
1360 **Figure 4.** Diurnal variations of oxidized aromatics including nitro-phenols
 1361 ($C_6H_5NO_3I^-$), nitro-benzenediols ($C_6H_5NO_4I^-$), methyl nitro-phenols ($C_7H_7NO_3I^-$),
 1362 methyl nitro-benzenediols ($C_7H_7NO_4I^-$), dinitro-phenols ($C_6H_4N_2O_5I^-$), dihydroxy
 1363 methyl benzoquinone ($C_7H_6O_4I^-$), tetrahydroxy toluene ($C_7H_8O_4I^-$), pentahydroxy
 1364 toluene and fragments of C9 aromatics ($C_7H_8O_5I^-$). The shaded areas indicate one
 1365 standard deviation.



1366

1367 **Figure 5.** (a) Correlation between particle-phase $C_6H_5NO_4I^-$ and $C_6H_{10}O_5I^-$. The
 1368 data points are color-coded using the time of the day. Solid and dash lines represent the
 1369 slopes during the nighttime and daytime, respectively. (b) Relative concentration of

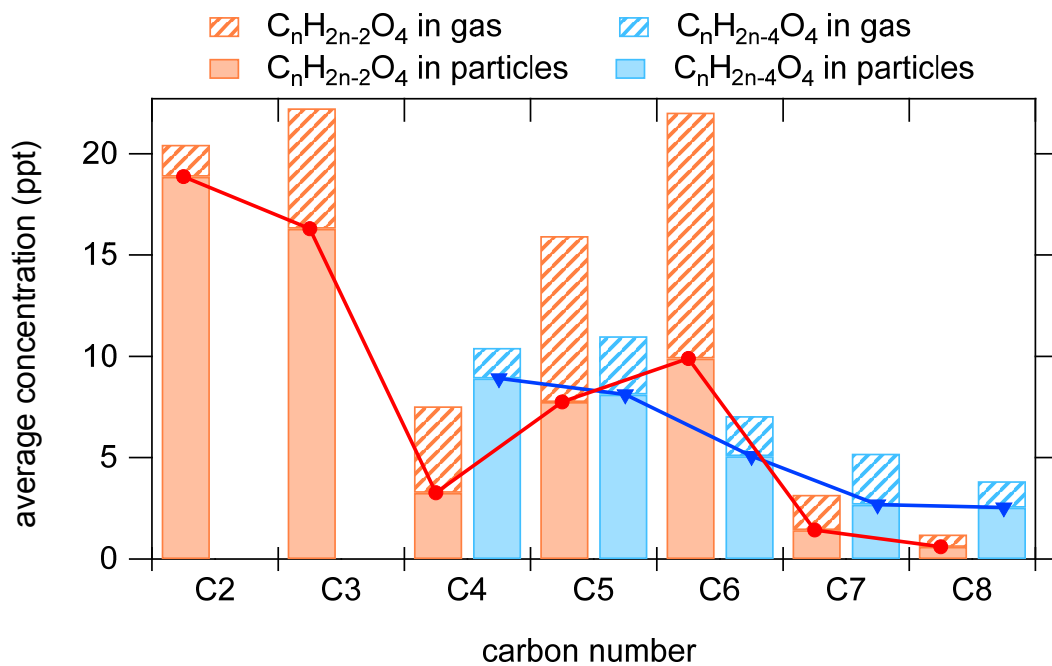
1370 $C_7H_8O_4I^-$ and $C_7H_7NO_3I^-$ in the gas phase as a function of NO_x concentration. The
1371 black line is the fitted curve using a double exponential function.



1372

1373 **Figure 6.** Diurnal variations of organic acids in the gas phase (red) and particle phase

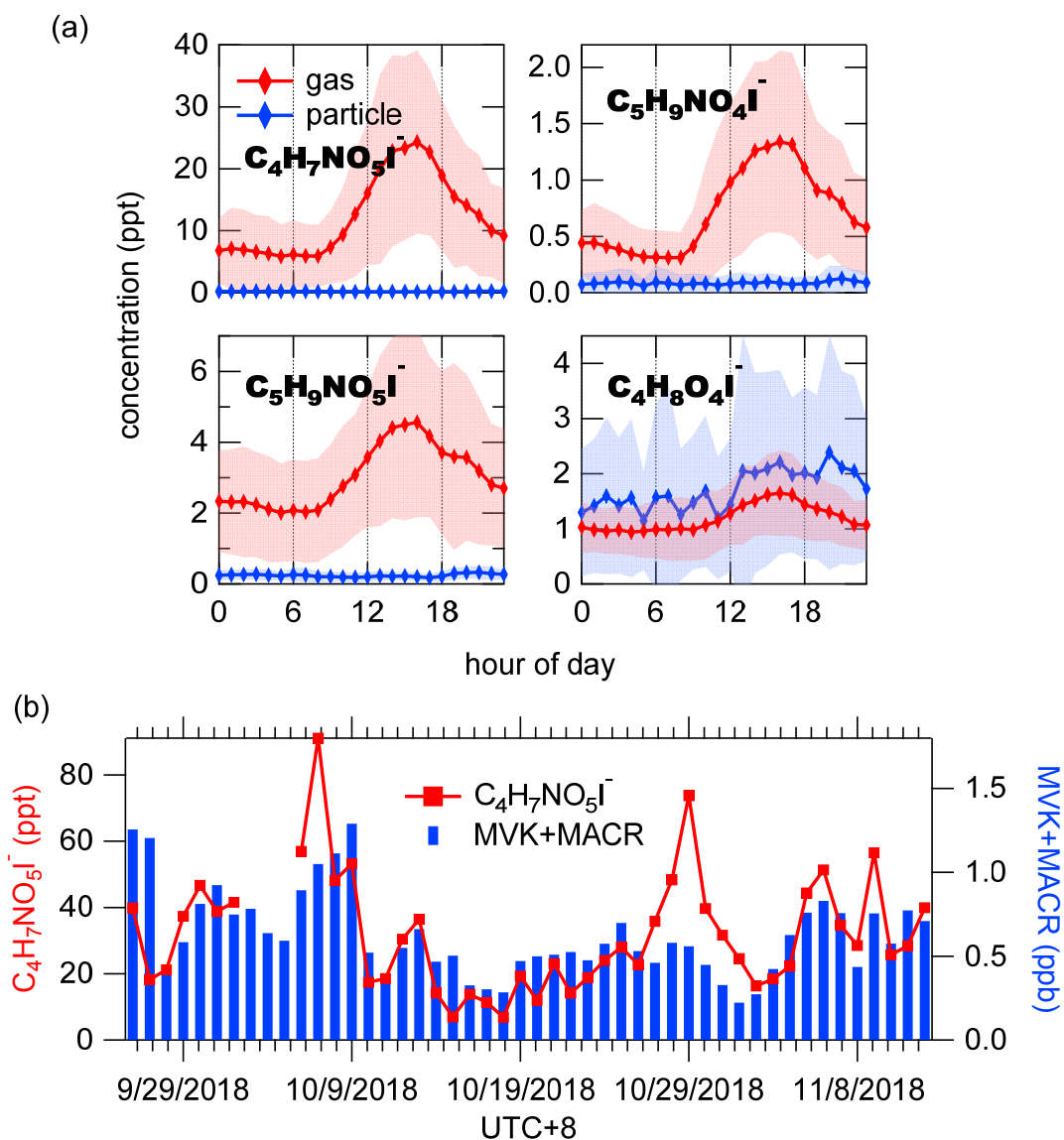
1374 (blue). The shaded area indicates one standard deviation.



1375

1376 **Figure 7.** Average concentrations of compounds with the formulas of $C_nH_{2n-2}O_4$

1377 and $C_nH_{2n-4}O_4$.



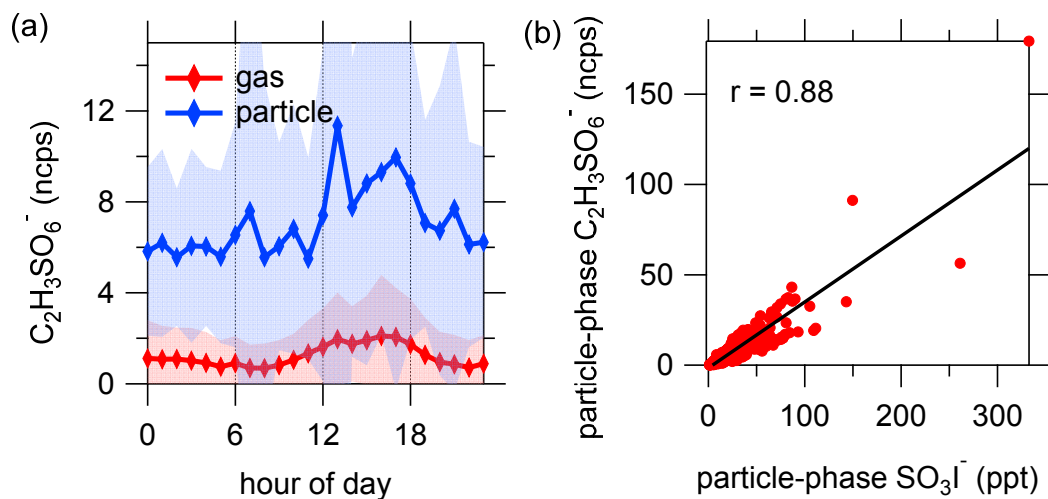
1378

1379 **Figure 8.** (a) Diurnal variations of isoprene oxidation products in the gas phase (red)

1380 and particle phase (blue). The shaded area indicates one standard deviation. (b) Time

1381 series of daily maximum concentrations of gaseous $C_4H_7NO_5I^-$ and MVK+MACR

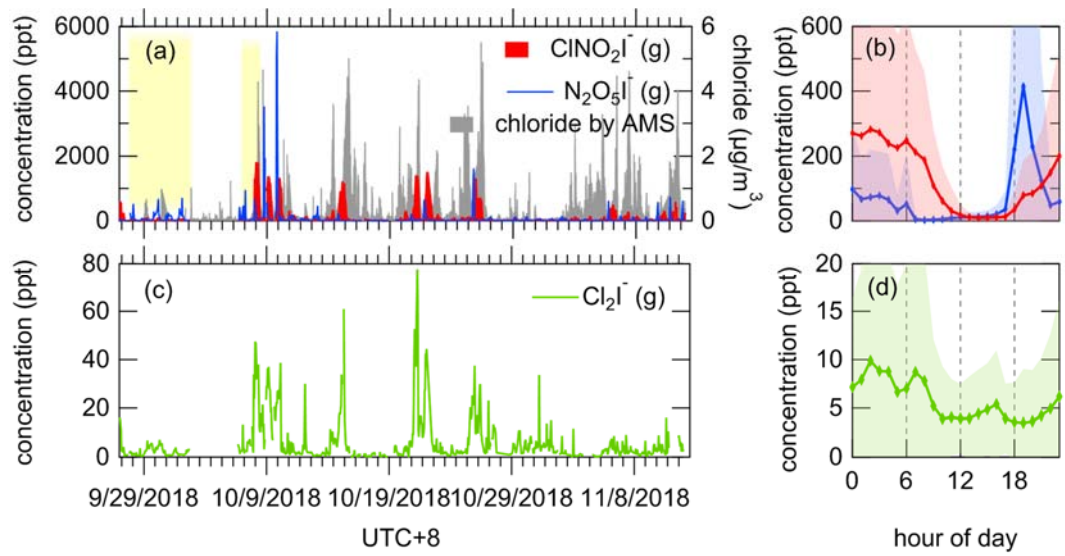
1382 ($C_4H_6OH^+$, m/z 71.05) measured by PTR-ToF-MS.



1383

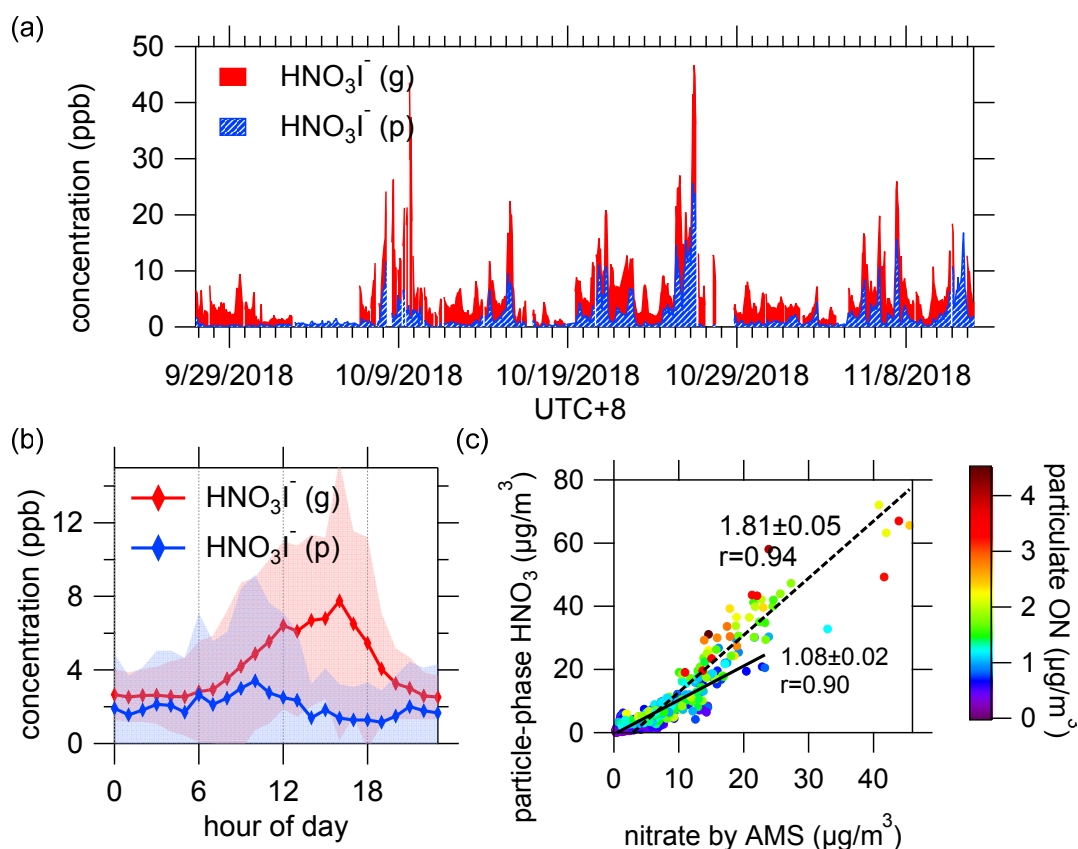
1384 **Figure 9.** (a) Diurnal variation of $C_2H_3SO_6^-$. The shaded areas indicate one standard

1385 deviation. (b) Correlation between particle-phase $C_2H_3SO_6^-$ and SO_3I^- .



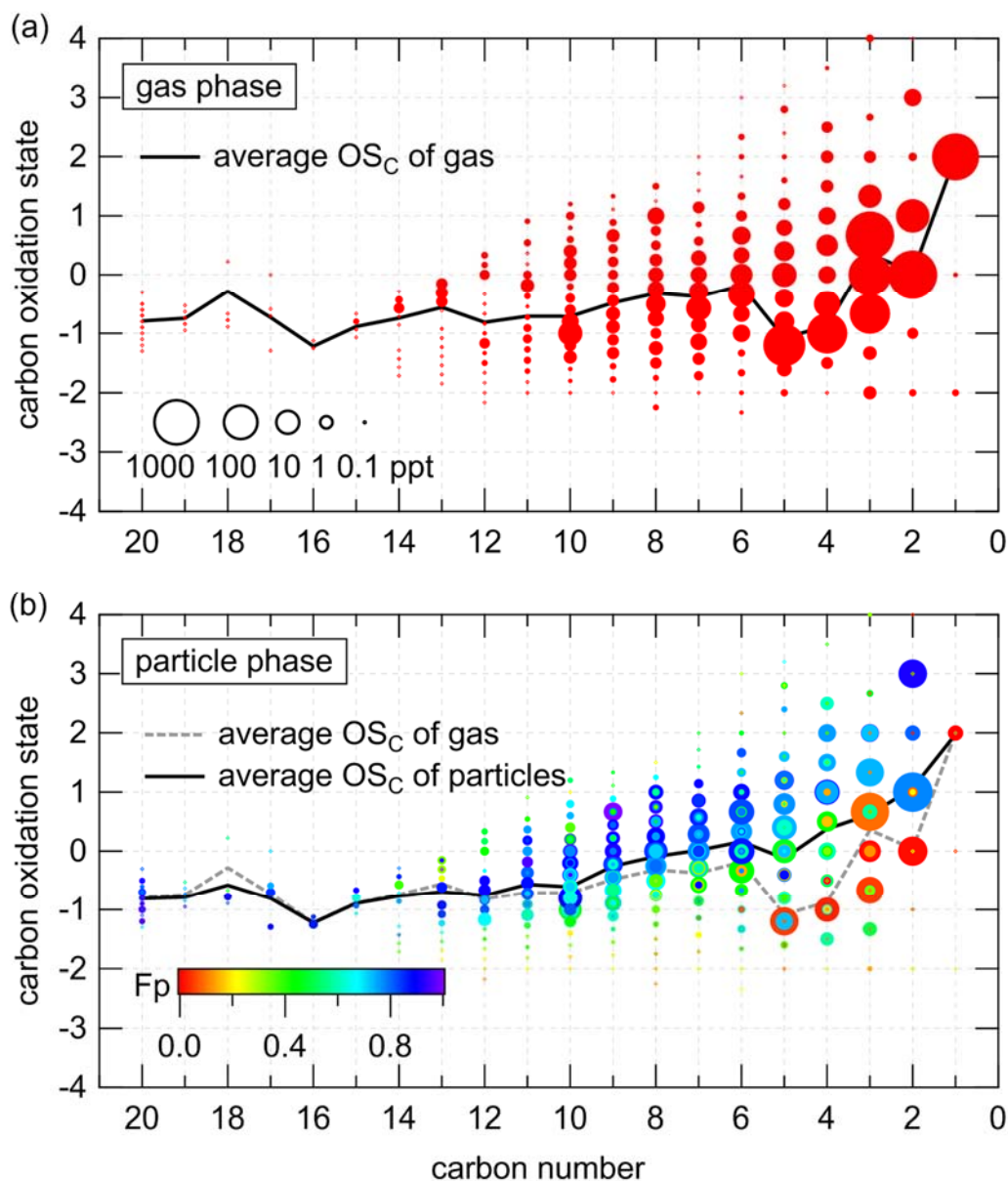
1386

1387 **Figure 10.** Time series and diurnal variations of humidity-corrected concentrations of
 1388 N_2O_5 and ClNO_2 (a, b) and Cl_2 (c, d). The tinted background indicates the days with
 1389 high concentrations of N_2O_5 but low concentrations of ClNO_2 . The shaded areas
 1390 indicate one standard deviation.



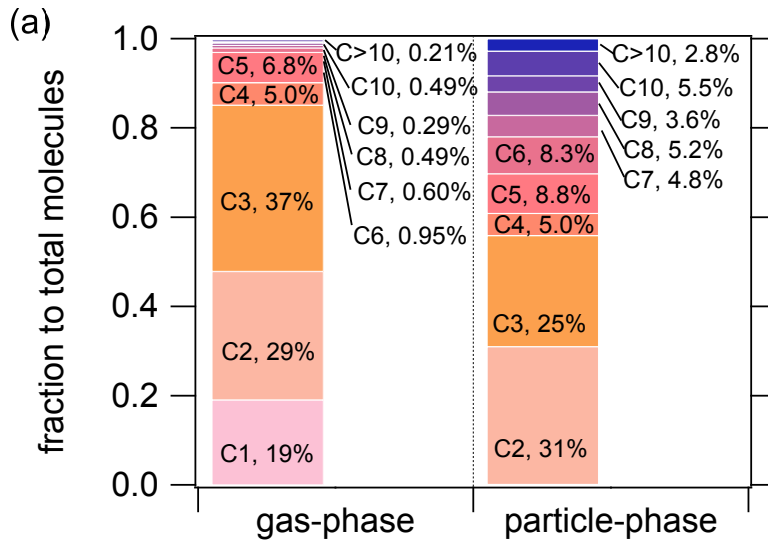
1392

1393 **Figure 11.** (a) Time series of humidity-corrected HNO_3I^- in both phases. (b) Diurnal
 1394 variation of humidity-corrected HNO_3I^- . The shaded areas indicate one standard
 1395 deviation. (c) Comparison of particle-phase HNO_3I^- and nitrate measured by AMS.
 1396 The color scale denotes particulate N-containing organic compounds measured by
 1397 FIGAERO-I-CIMS (pON). The solid and dash lines show the fitted results for the
 1398 dataset of pON less than $1 \mu\text{g}/\text{m}^3$ and more than $1 \mu\text{g}/\text{m}^3$, respectively. The
 1399 concentration of gaseous HNO_3I^- shown here only included the last 5-minute of
 1400 every gas-phase working mode, as high level of HNO_3 came out of aerosol which then
 1401 passed through the CIMS in a short time during particle analysis and a substantial
 1402 amount would subsequently accumulate on the inner surfaces, leading to a persistent
 1403 carried over signal that was long enough to disturb the next gas measurement cycle
 1404 (Palm et al., 2019).

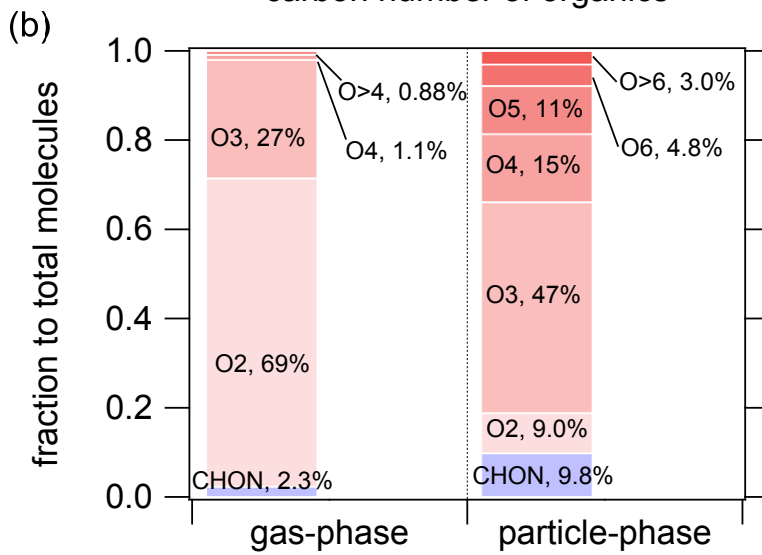


1405

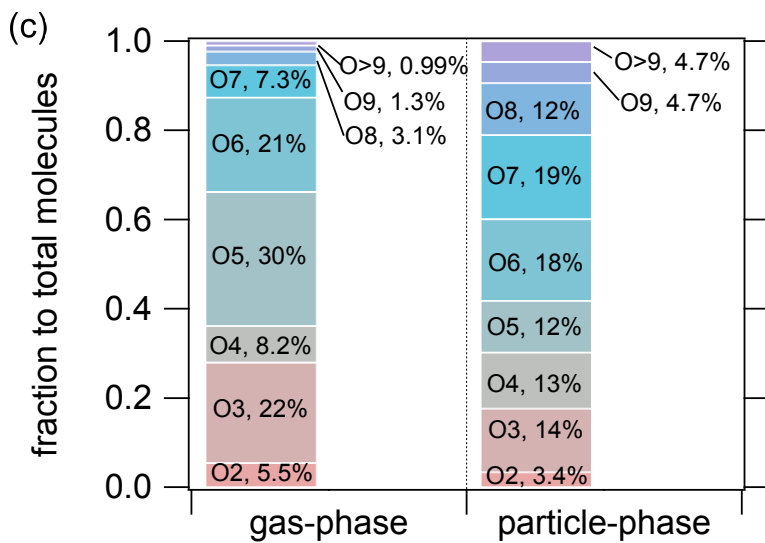
1406 **Figure 12.** $\overline{OS}_C - n_C$ spaces for $C_xH_yO_z$ and $C_xH_yN_{1,2}O_z$ compounds in gas-phase
 1407 (a) and particle-phase (b). The diameters of circles are proportional to the logarithmic
 1408 average concentrations. The black lines are the average \overline{OS}_C of each carbon number
 1409 for compounds in gas-phase and particle-phase, respectively. The compounds in Fig. (b)
 1410 are color-coded by their fractions in particles.



carbon number of organics

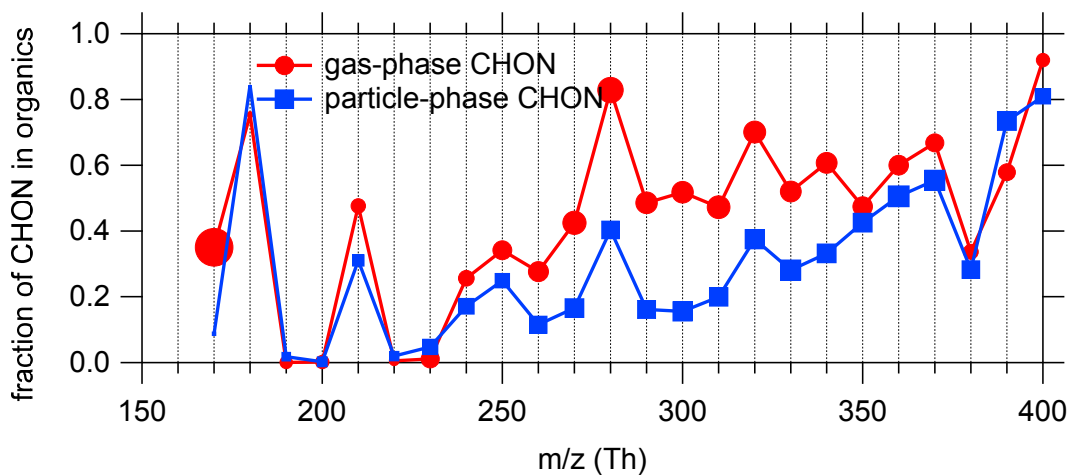


oxygen number of organics



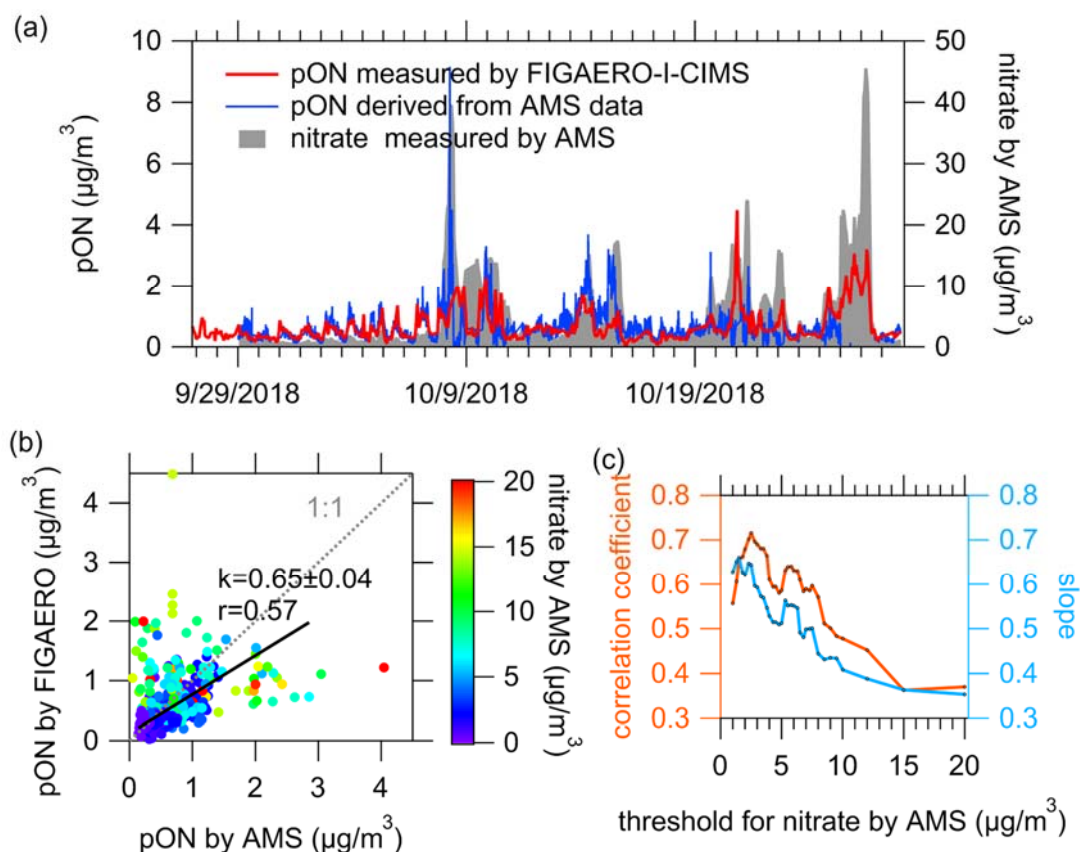
oxygen number of CHON

1412 **Figure 13.** Carbon number distribution (a) and oxygen number distribution of total
1413 $C_xH_yO_z$ and $C_xH_yN_{1,2}O_z$ compounds (b), and oxygen number distribution of
1414 $C_xH_yN_{1,2}O_z$ compounds (c).



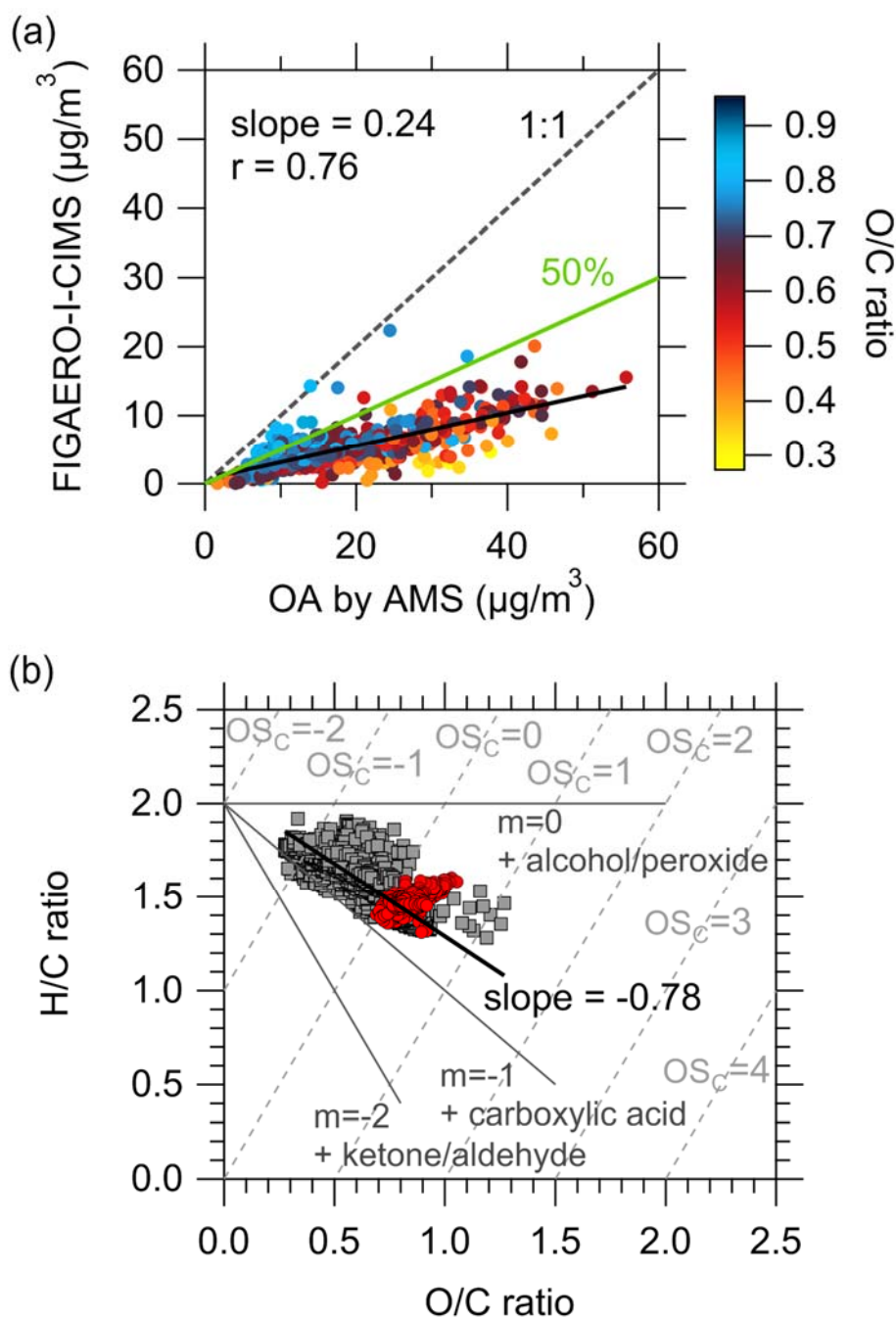
1415

1416 **Figure 14.** The average fractions of CHON to total organic compounds (CHO + CHON
 1417 + CHOS + CHONS) of every 10 Th in both phases. See Fig. S16 for the overall
 1418 distribution of the contributions of species classes to the total concentrations. Marker
 1419 sizes indicate the total concentration level in each m/z bin. High ambient concentration
 1420 of HNCO resulted in the large marker around m/z 170 in the gas phase (Wang et al.,
 1421 2020d).



1423

1424 **Figure 15.** (a) Time series of particulate N-containing organic compounds measured by
 1425 FIGAERO-I-CIMS (pON by FIGAERO), particulate organic nitrates derived from
 1426 AMS data (pON by AMS) as well as particulate inorganic nitrate. (b) Comparison of
 1427 pON by FIGAERO and pON by AMS, color-coded by the concentrations of particulate
 1428 inorganic nitrate measured by AMS. The black line presents the linear fit for nitrate by
 1429 AMS below 8 µg/m³. (c) The determined slopes and correlation coefficients between
 1430 pON by FIGAERO versus pON by AMS by filtering the data below different thresholds
 1431 of particulate inorganic nitrate measured by AMS.



1432

1433 **Figure 16.** (a) Comparison of particulate organic compounds measured by the
 1434 FIGAERO-I-CIMS and AMS, color-coded by O/C ratios measured by AMS. The black
 1435 line is the slope which represents the fraction of OA explained by the measurements of
 1436 FIGAERO-I-CIMS. The green line shows the results from previous work which were
 1437 ~50% (Lopez-Hilfiker et al., 2016; Stark et al., 2017). (b) Van Krevelen diagrams for
 1438 organic aerosol derived from AMS data (gray squares) and FIGAERO-I-CIMS data (red
 1439 circles). Black line is the slope of AMS data. Gray dotted lines are estimated carbon
 1440 oxidation state.